Advances in Materials Science and Engineering

Concrete and Structure with Recycled Aggregate

Guest Editors: Alex Li, François Buyle-Bodin, Yves Delmas, Dimitar Dontchev, and Christophe Petit

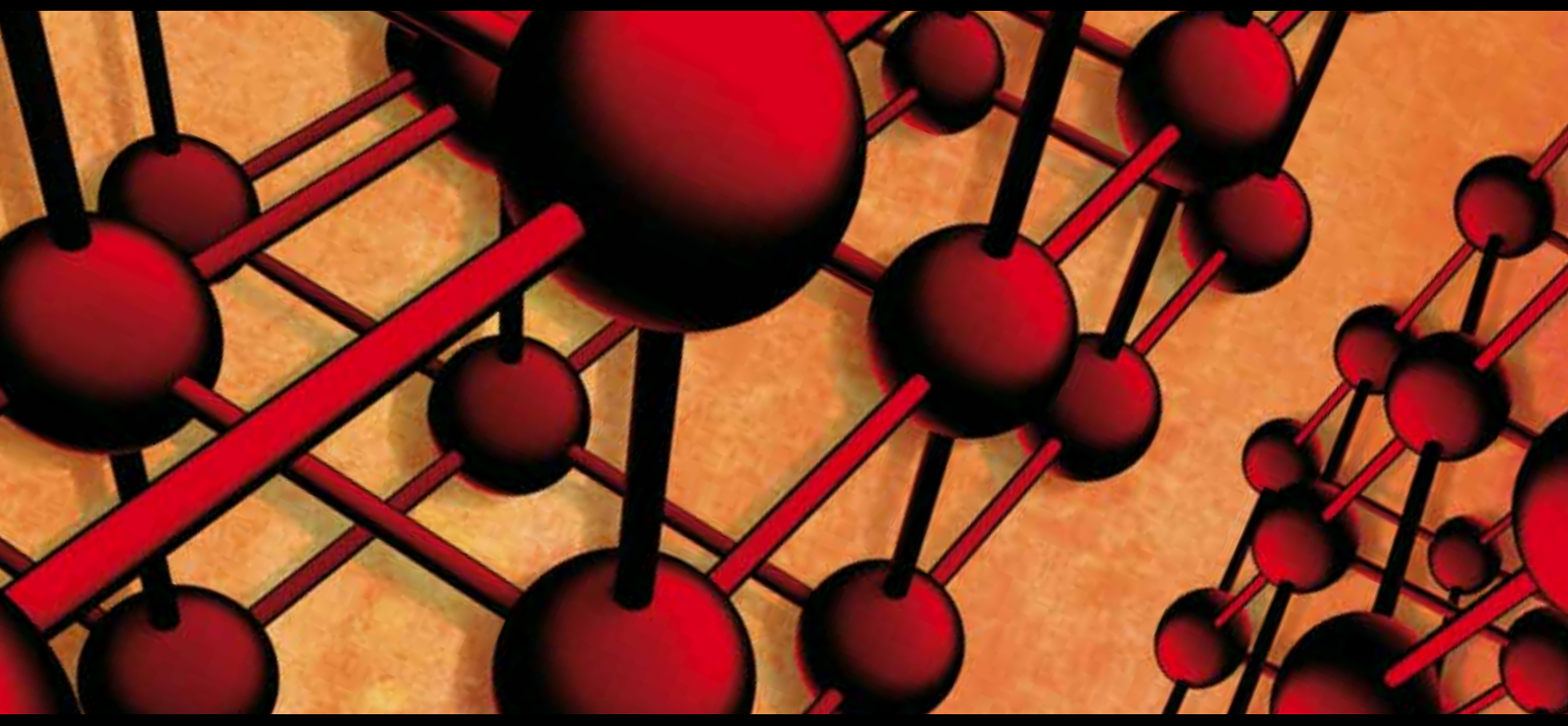

Concrete and Structure with Recycled Aggregate

Advances in Materials Science and Engineering

Concrete and Structure with Recycled Aggregate

Guest Editors: Alex Li, François Buyle-Bodin, Yves Delmas, Dimitar Dontchev, and Christophe Petit

Editorial Board

Contents

Hindawi Publishing Corporation
Advances in Materials Science and Engineering
Volume 2013, Article ID 328036, 1 page
http://dx.doi.org/10.1155/2013/328036

Editorial
Concrete and Structure with Recycled Aggregate

Alex Li,[1] François Buyle-Bodin,[2] Yves Delmas,[1] Dimitar Dontchev,[3] and Christophe Petit[4]

[1] *Laboratory of Civil Engineering, Université de Reims Champagne-Ardenne, 51687 Reims, France*
[2] *UFR of Geography and Management, Université de Lille 1 Sciences et Techniques de Lille, 59100 Lille, France*
[3] *University of Chemical Technology and Metallurgy Sofia, 1756 Sofia, Bulgaria*
[4] *Department of Civil Engineering, Université de Limoges, 19300 Egletons, France*

Correspondence should be addressed to Alex Li; alex.li@univ-reims.fr

Received 1 December 2013; Accepted 1 December 2013

In recent years, importance and necessity of using the recycled aggregate are recognized because of the depletion of quality primary aggregates and greater awareness of environmental protection. It is now widely accepted that there is a significant potential for reclaiming and recycling demolished debris for use in value added applications to maximize economic and environmental benefits. There is increasing demand and interest in aggregates from non-traditional sources such as from industrial byproducts and recycled construction and demolition wastes. The purpose of this special issue is to summarize the various researches on concrete and structure with recycled aggregate. A few papers invited in this special issue give their contribution to advance research in this field.

The first paper of this special issue presents the cellular concrete bricks obtained by using a lightweight mortar with recycled expanded polystyrene aggregate instead of sandy materials. This type of concrete bricks is lighter and more flexible, which makes it less vulnerable to cracking walls due to soil displacements. The developed bricks have good mechanical properties and flexural strength and less permeable.

The second paper deals with the cementing potential of pulverized oyster shell, rich in calcium, when mixed with fly ash and soil. Authors indicate that more the pulverized oyster shell adds, lower the strength will get both in the soil and lime specimen. The soil specimens containing fly ash gradually gain strength as curing proceeds.

The third paper shows that the impact properties of the recycled aggregate concrete exhibit strong strain-rate dependency and increase the increase of peak strain-rate. The transition point from low strain-rate sensitivity to high sensitivity decreases with the increase of matrix strength. Authors indicate that the energy absorption capacity of recycled aggregate concretes specimens is lower than that of natural aggregate concretes.

The fourth paper presents an optimization of the mixing proportion of recycled aggregate concrete by using neural networks based on genetic algorithms. This method will contribute to improve the usage of the recycled aggregate in the construction industry and to reduce the waste in the construction process.

In the fifth paper, the effects of ground waste concrete powder coming from the attached paste/mortar on water demand for normal consistency, setting time, fluidity, and compressive strength of cement were analyzed.

The last paper presents the fire resistance and the relevant thermal properties of high-performance concrete (HPC) with fly ash. The effect of temperature from 200 to 500°C on compressive strength, cubic compressive strength, cleavage strength, flexural strength, and the ultrasonic velocity of the high-performance concrete with fly ash was studied.

Alex Li
François Buyle-Bodin
Yves Delmas
Dimitar Dontchev
Christophe Petit

Hindawi Publishing Corporation
Advances in Materials Science and Engineering
Volume 2013, Article ID 160162, 5 pages
http://dx.doi.org/10.1155/2013/160162

Research Article

Cellular Concrete Bricks with Recycled Expanded Polystyrene Aggregate

Juan Bosco Hernández-Zaragoza,[1] Teresa López-Lara,[1] Jaime Horta-Rangel,[1] Carlos López-Cajún,[1] Eduardo Rojas-González,[1] F. J. García-Rodríguez,[2] and Jorge Adue[3]

[1] *Universidad Autónoma de Querétaro, Facultad de Ingeniería, Cerro de las Campanas S/N, Col. Las Campanas, 76010, QRO, Mexico*
[2] *Instituto Tecnológico de Celaya, Departamento de Ingeniería Industrial, Avenida García Cubas 1200 Esquina Ignacio Borunda, 38010 Celaya, GTO, Mexico*
[3] *Universidad Nacional de Rosario, Instituto de Mecánica Aplicada y Estructura (IMAE), Facultad de Ciencias Exactas, Ingeniería y Agrimensura, Riobamba y Berutti S/N, 2000 Rosario, Argentina*

Correspondence should be addressed to Teresa López-Lara; lolte@uaq.mx

Received 20 May 2013; Revised 2 October 2013; Accepted 16 October 2013

Academic Editor: Alex Li

Cellular concrete bricks were obtained by using a lightweight mortar with recycled expanded polystyrene aggregate instead of sandy materials. After determining the block properties (absorption, compressive strength, and tensile stresses), it was found that this brick meets the requirements of the masonry standards used in Mexico. The obtained material is lighter than the commercial ones, which facilitates their rapid elaboration, quality control, and transportation. It is less permeable, which helps prevent moisture formation retaining its strength due to the greater adherence shown with dry polystyrene. It was more flexible, which makes it less vulnerable to cracking walls due to soil displacements. Furthermore, it is economical, because it uses recyclable material and has properties that prevent deterioration increasing its useful life. We recommend the use of the fully dry EP under a dry environment to obtain the best properties of brick.

1. Introduction

A lightweight mortar can be produced in different ways and basically depends on the air factor, that is, decreasing the density of a material consists in including air in its structure, which can be done by replacing the coarse aggregate (sand) by air. Thus, the air inclusion in the material structure favors the formation of bubbles (empty space) inside the concrete or mortar. Therefore, when it dries out, the air holes generate a lightweight material. This type of concrete is known as *Cellular Concrete*. It has been suggested to define a lightweight concrete as a concrete made with lightweight aggregate or without aggregates that allow to obtain a weight less than conventional concrete of 2400 kg/m^3 [1].

With regard to the use of the polystyrene in concretes, literature mentions the use of expanded polystyrene (EP) beads as lightweight aggregate both in concretes and mortars containing silica fume a supplementary cementitious material. The resulting concretes were seen to have densities varying from 1500 to 2000 kg/m^3, with the corresponding strengths varying from 10 to 21 MPa [2]. Another study covers the use of expanded polystyrene (EPS) and unexpanded polystyrene (UEPS) beads as lightweight aggregate in concretes that contain fly ash as a supplementary cementitious material. Lightweight concrete with wide range of concrete densities (1000–1900 kg/m^3) were studied mainly for compressive strength, split tensile strength, moisture migration, and absorption. The results indicate that for comparable aggregate size and concrete density, concrete with UEPS aggregate exhibited 70% higher compressive strength than EPS aggregate [3].

Fine silica fume greatly improved the bond between the EP beads and cement paste and increased the compressive strength of EP concrete. The research showed that EPS concrete with a density of 800–1800 kg/m^3 and a compressive strength of 10–25 MPa can be made by partially replacing

coarse and fine aggregate by EPS beads. In addition, adding steel fiber significantly improved the drying shrinkage [4].

Another investigation shows the comparison between the mechanical properties of EP concretes containing fly ash with the literature results on concretes containing ordinary Portland cement alone as the binder [5]. A research proposes the development of a class of structural grade polystyrene aggregate concrete with a wide range of concrete densities between 1400 and 2100 kg/m^3 through partial replacement of coarse aggregate with polystyrene aggregate in control concrete [6].

Styrene-butadiene rubber latex as a polymeric admixture was applied in lightweight expanded polystyrene (EP) concrete. The effects of curing conditions and polymer-cement ratio on the compressive and flexural strengths of polymer-modified EP concretes were investigated [7]. Hardened concrete containing chemically treated expanded polystyrene beads showed that the strength, stiffness, and chemical resistance of polystyrene aggregate concrete of a constant density were affected by the water to cement ratio [8].

In the first part of this research, based on the definition and characteristics of a lightweight concrete, a low-density recyclable material was searched, such that could be recycled using a cheap sustainable recycling method. This material was the *expanded polystyrene* (EP). With this material, it a mortar was produced in which the coarse aggregates were substituted completely by low-density particles. So, bricks are composed of recycled expanded polystyrene as aggregate and commercial Portland cement as binder. Unlike most of the works published in the literature, this mortar does not use pozzolans or additives or additional aggregates. In this previous study, this material had a good adherence with the hydrated cement and the best mechanical properties in the cellular concrete were obtained for a water/cement ratio of 0.4 and 600 g of expanded polystyrene [9].

In the second stage, the core of this research, and with the defined technology, a specific technological application of the mortar of recycled material was the making of cellular bricks. These should be competitive on price, quality, and mechanical and physical properties against the current ones on the market. Furthermore, the cellular bricks should use a recyclable material in a sustainable fashion.

2. Methods and Techniques

The activities listed below allowed the fabrication and the mechanical and physical evaluation of the cellular-concrete bricks;

(i) getting and milling of the EP;

(ii) application of the water/cement ratio of 0.4;

(iii) realization of the cellular concrete;

(iv) fabrication of bricks using steel molds of 6×10×20 cm;

(v) unmolding and obtaining the dry-weight of the bricks;

(vi) absorption, Compressive, and Tensile tests; ASTM C67-03a Standard includes the three tests [10];

(vii) report of results;

(viii) comparison of the results with the reported values of some commercial bricks in Mexico.

Compressive strength of expanded polystyrene (EPS) lightweight concrete increases significantly with a decrease in EPS bead size [11, 12]. Adding, another study includes three sizes of polystyrene particles (1, 2.5, and 6.3 mm) in concrete and concludes that the size of 1 mm has greater resistance to compression [12]. Then, as the goal of the project was to reuse a recyclable material such as expanded polystyrene, the particle sizes depended on the sustainable and cheap milling process. In fact, the sizes achieved (2–4 mm) were very close to those reported as greater compressive strength [12].

In first place, the search of EP waste materials was carried out. These EP residuals were from items obtained mainly from computers packing. Once the material was collected, it was milled with water in a kitchen blender, because without water there was no milling. Resulting particle size was 2–4 mm. Then, the excess of water was eliminated and EP was dried at the natural environment, without using ovens.

In agreement with previous studies, the cellular concrete was obtained by mixing 600 g of polystyrene and a water/cement ratio of 0.4. The cement used was a CPC (composite Portland cement).

It should be pointed out that one of the important factors that influenced this research was the high environmental humidity in the place where this research was realized (Rosario, Argentina). This fact led to the result of a fluid composite that allowed easily the filling of the steel molds.

Two types of specimens, labeled as A and B with dimensions of 100 × 200 × 60 mm, were tested. Type A had a water/cement ratio of 0.4, a weight of 0.600 Kg of EP in semihumid state, and an age of 28 days. Type B had the same water/cement ratio, but with 0.520 Kg weight of semidry EP. The B test age was only 14 days because of the end of the project.

Due to environmental humidity circumstances, when we dry the wet polystyrene (resultant material for milling process) to 7 days, we obtained weights of 600 g for bricks A and B. Immediately we elaborate the bricks A (with 600 g) in the first stage of the project. Then, as the remaining polystyrene was used 28 days later, we noticed that the weight had decreased. Therefore this remaining material was divided and used in five bricks B. So the bricks B had 520 g of polystyrene. Therefore bricks A were prepared with "semihumid" polystyrene and bricks B with "semidry" polystyrene. We did not obtain a fully dry weight of EP because of the condition of environmental local dampness.

Environmental humidity levels for "semihumid" and "semidry" polystyrene were the same; the difference was the exposure time under those conditions. Environmental humidity of the place was 62–95% [14] in the days of the experiment (Rosario, Argentina; August 2012). The polystyrene named "semihumid" was exposed 7 days under this environment and 28 days for the "semidry."

After 27 days for bricks A and 13 days for bricks B, the absorption test was performed to the bricks (this experimental test requires 24 h [10] of saturation of the bricks for

Table 1: Statistical evaluation of absorption (%), Compressive and tensile strength (MPa) of A and B.

Property	Number of data	Mean	Median	Variance	Standard deviation	Coefficient of variation, %
Absorption, A	6	9.328	9.135	0.842	0.917	9.84
Absorption, B	6	4.464	4.21	0.284	0.533	11.95
Compressive strength, A	5	9.69	9.3	0.840	0.916	9.46
Compressive strength, B	5	6.916	7.28	0.598	0.773	11.18
Tensile strength, A	6	2.195	2.22	0.254	0.503	22.95
Tensile strength, B	5	1.632	1.64	0.002	0.046	2.85

its evaluation). Therefore, the absorption test results were obtained at 28 days for bricks A and at 14 days for bricks B with the Compressive and Tensile tests.

Theoretically, if kept in a moist environment, about 90% of its strength is gained in the first 28 days. The main criterion for evaluating the compressive strength of concrete is the strength of the concrete on 28th day. The concrete sample is tested after 28 days and the result of this test is considered as a criterion for quality and rigidity of that concrete [15].

3. Results and Discussion

Statistical evaluation of the percentage of absorption of A and B are shown in Table 1. For measuring the absorption property, the ASTM C67-03a standard specifies that the material is kept immersed in water for 24 hours [10]. The percentage of absorption was determined by (1) [10]. Dry and saturated weights (W_d and W_s, resp.) of the brick were before and after its saturation, respectively:

$$\%\ \text{Absorption} = 100\frac{(W_s - W_d)}{W_d}. \quad (1)$$

From Table 1 we observed that brick B (semidry EP) has less absorption than brick A (semihumid EP). Although the time of study of brick B is half of A, the trend to increase absorption is very little. Thus, it is apparent that this material could diminish the moisture generated in walls built with other types of bricks, which the absorption is greater due to the type of aggregates being used, such as sand.

Statistical results of the compressive tests [10] to both types of specimens, of area 100 × 200 mm, are shown in Table 1. It should be recalled that bricks A were 28 days old, whereas bricks B were 14 days old. Because of the above, the differences in strength could be justified. It can also be observed that the trend in the increase of strength continues in specimens B, and it is would overcome the value reached by specimens of the type A, due to the greater adherence (less absorption) created by the semidry EP.

The tensile strength or Modulus of Rupture [10] was computed as

$$S = \frac{3W\,(L/2 - x)}{bd^2}, \quad (2)$$

where S is tensile strength or Modulus of Rupture (MPa), W is applied maximum load (kg), L is distance between supports (cm) (computed as the specimen length minus 2 inches, because the supports are at distance of 1 inch from each end), x is horizontal distance from the point of application of the load to the place where the fissure arises (cm), and b and d are width and thickness of the specimen, respectively (cm).

Statistical results of the Tensile test of specimen types A and B are shown in Table 1. These were determined from (2).

From Table 1 the Mean of tensile strength for specimens A and B are 2.195 and 1.632 MPa, respectively. Specimen type B showed a partial tensile strength with relation to the one that can develop in 28 days.

Assuming traditional concrete bricks with coarse aggregates and burned clay bricks have very low values of tensile strength, approximately 0.8 MPa in average [13]. Thus, EP provides flexural properties to the brick that contribute to wall stability, especially when it has ascending and descending movements caused by problematic soils such as expansive and collapsible soils, phreatic water level changes, and earthquakes, among others. Therefore, this material reduces the appearance of cracks in the wall. This aspect had not been considered in the fabrication of traditional bricks.

Concrete can hardly be considered to be homogeneous because the properties of its constituents are different and it is, to some extent, anisotropic. Nevertheless, the fracture mechanics approach helps to understand the mechanism of failure of concrete. The actual failure paths usually follow the interfaces of the largest aggregate particles and cut through the cement paste, and occasionally also through the aggregate particles themselves [16].

As in the concrete, the failure paths usually follow the interfaces of the polystyrene aggregate particles and cut through the cement paste and the aggregate particles themselves. Under compression, the cracks are approximately parallel to the applied load but some cracks form at an angle to the applied load (Figure 1). The parallel cracks are caused by a localized tensile stress in a direction normal to the compressive load; the inclined cracks occur due to collapse caused by the development of shear planes. It should be noted that the fracture patterns of Compression test are for direct stresses only [16].

In the flexure test, the maximum tensile stress is reached in the bottom fibre of a test beam so the cracks are vertical and are near the point of application of the load (Figure 2). In the Tensile test, the top surface is subjected to a compression state, while the lower surface is subjected to traction. The concentration of stress at the crack tip is, in fact, three-dimensional but the greatest weakness is when the orientation of a crack is normal to the direction of the applied load.

Table 2: Comparative properties of specimen A and B versus reported parameters.

Property	Brick A	Brick B	Burned clay brick [13]	Mortar brick [13]
Dimensions: thick, width, and length (cm)	6, 10, 20	6, 10, 20	5.5, 11.5, 23	18, 12, 38
Volumetric weight (kg/m^3)	1568	1236	1580	1890
Average absorption (%)	9.3	4.3	17.8	25.2
Compressive strength (MPa)	9.69	6.92	11.16	4.69
Average rupture stress (MPa)	2.94	1.65	0.755	0.794

Figure 1: Resulting cracks in the brick under Compression test.

Figure 2: Resulting cracks in the brick under Tensile test.

In a truly brittle material (uniform distribution stress), the energy released by the onset of crack propagation is sufficient to continue this propagation, because, as the crack extends, the maximum stress increases and the brittle fracture strength decreases. In consequence, the process accelerates. In the case of nonuniform stress (e.g., in flexure), the propagation of a crack is blocked, additionally, by the surrounding material at a lower stress [16].

Table 2 shows the results of the properties obtained in the specimens. These are compared with parameters reported elsewhere [13]. This table shows that the EP brick is lighter than the other ones, which facilitates their elaboration, production, and transportation. Then, this material has the property of low absorption, which helps to prevent possible moisture in walls. Besides, this material is resistant, since its compressive strength (with semidry EP) is similar to the reported maximum commercial ones, which could possibly exceed using the EP in dry condition. Finally, this material can be four times more flexible than some commercial blocks, which makes it less vulnerable to possible cracks in walls caused by ascending or descending movements of the underlying soil.

The relatively high values of the coefficient of variation (Table 1) in the test depended on the type of test and the number of data. Absorption and Compression test have similar values of the coefficient of variation; that is, we see the same range of error when performing the test, which can be decreased by increasing the number of tests. Then, Tensile test shows two very different coefficients of variation mainly due to the completion of the test that requires great precision and care. In this test we noticed that the specimen A has greater error than B because A was tested first. However, all the data of all properties were higher than the reference values in Table 2.

Both materials (A and B) do not have the same time and amount of polystyrene. The specimen A has the complete initial variables and B does not. Therefore they cannot be comparable between them. So, in this work we report and analyze the properties acquired in the specimen A and then, the properties acquired in the specimen B (with reference to the specimen A) because even though this material has its incomplete initial variables becomes significant properties precisely because of this situation. Finally both specimens were better than the reference materials in Table 2.

4. Conclusions

The brick developed in this research showed efficient mechanical properties and it could be used as masonry in construction since this material meets the required parameters. It composed of recycled expanded polystyrene as aggregate and commercial Portland cement as binder. Unlike most of the works reported in the literature, this mortar does not use pozzolans or additives or additional aggregates.

Unlike concrete (with coarse aggregate), the failure paths always follow the interfaces of the polystyrene aggregate particles and cut through the cement paste and the aggregate particles themselves. The polystyrene brick cracks are similar to reported concrete cracks in the Compression and Tensile test.

In the results of the properties we observed the same range of error when performing the tests, which can be decreased by increasing the number of tests.

Sustainable use of expanded polystyrene in cellular concrete bricks was very favorable regarding to those existing in the market. The obtained material is lighter, which facilitates

its production and transportation and is less permeable, which helps to avoid moisture formation keeping its strength. In addition, it is more resistant as well as flexible, which makes it less vulnerable to cracking walls caused by ground movements. Finally, this material is cheaper because it uses recyclable material and has properties that prevent its deterioration increasing its lifetime.

We observe that the environmental moisture and EP moisture diminished the resistance properties of brick and increased its density and absorption. We recommend the use of the fully dry EP under a dry environment to obtain the best properties of brick.

References

[1] S. Chandra and L. Berntsson, *Lightweight Aggregate Concrete. Science, Technology and Applications*, Noyes Publications, New York, NY, USA, 2003.

[2] K. G. Babu and D. S. Babu, "Behaviour of lightweight expanded polystyrene concrete containing silica fume," *Cement and Concrete Research*, vol. 33, no. 5, pp. 755–762, 2003.

[3] D. S. Babu, G. K. Babu, and W. Tiong-Huan, "Effect of polystyrene aggregate size on strength and moisture migration characteristics of lightweight concrete," *Cement and Concrete Composites*, vol. 28, no. 6, pp. 520–527, 2006.

[4] B. Chen and J. Liu, "Properties of lightweight expanded polystyrene concrete reinforced with steel fiber," *Cement and Concrete Research*, vol. 34, no. 7, pp. 1259–1263, 2004.

[5] D. S. Babu, G. K. Babu, and W. Tiong-Huan, "Properties of lightweight expanded polystyrene aggregate concretes containing fly ash," *Cement and Concrete Research*, vol. 35, no. 6, pp. 1218–1223, 2005.

[6] W. C. Tang, Y. Lo, and A. Nadeem, "Mechanical and drying shrinkage properties of structural-graded polystyrene aggregate concrete," *Cement and Concrete Composites*, vol. 30, no. 5, pp. 403–409, 2008.

[7] B. Chen and J. Liu, "Mechanical properties of polymer-modified concretes containing expanded polystyrene beads," *Construction and Building Materials*, vol. 21, no. 1, pp. 7–11, 2007.

[8] R. Sri Ravindrarajah and A. J. Tuck, "Properties of hardened concrete containing treated expanded polystyrene beads," *Cement and Concrete Composites*, vol. 16, no. 4, pp. 273–277, 1994.

[9] O. García-Díaz, *Mortero de baja densidad con poliestireno reciclado [M.S. thesis]*, Facultad de Ingeniería, Universidad Autónoma de Querétaro, Querétaro, México, 2011.

[10] "Standard test methods for sampling and testing brick and structural clay tile," ASTM C67-03a, Annual Book of ASTM Standards, 2003.

[11] A. Laukaitis, R. Žurauskas, and J. Keriene, "The effect of foam polystyrene granules on cement composite properties," *Cement and Concrete Composites*, vol. 27, no. 1, pp. 41–47, 2005.

[12] K. Miled, K. Sab, and R. le Roy, "Particle size effect on EPS lightweight concrete compressive strength: experimental investigation and modelling," *Mechanics of Materials*, vol. 39, no. 3, pp. 222–240, 2007.

[13] A. Tena, A. Juárez, and V. H. Salinas, "Resistencia y deformación de muros de mampostería combinada y confinada sujetos a cargas laterales," *Revista de Ingeniería Sísmica*, vol. 76, pp. 29–60, 2007.

[14] WeatherOnline Ltd, 1999—2013, Weather in Rosario, Argentina, August 2012, http://www.woespana.es.

[15] V. K. Alilou and M. Teshnehlab, "Prediction of 28-day compressive strength of concrete on the third day using artificial neural networks," *International Journal of Engineering*, vol. 3, no. 6, pp. 565–576, 2010.

[16] A. M. Neville and J. J. Brooks, *Concrete Technology*, Prentice Hall, 2nd edition, 2010.

Hindawi Publishing Corporation
Advances in Materials Science and Engineering
Volume 2013, Article ID 527089, 10 pages
http://dx.doi.org/10.1155/2013/527089

Research Article

Optimizing the Mixing Proportion with Neural Networks Based on Genetic Algorithms for Recycled Aggregate Concrete

Sangyong Kim,[1] Hee-Bok Choi,[2] Yoonseok Shin,[3] Gwang-Hee Kim,[3] and Deok-Seok Seo[4]

[1] *School of Construction Management and Engineering, University of Reading, Reading RG6 6AW, UK*
[2] *Department of Architectural Engineering, Jeju National University, Jeju 690-756, Republic of Korea*
[3] *Department of Plant & Architectural Engineering, Kyonggi University, Gwanggyosan-Ro, Yeongtong-Gu, Suwon-Si, Gyeonggi-Do 443-760, Republic of Korea*
[4] *Department of Architectural Engineering, Halla University, Wonju-Si 220-712, Republic of Korea*

Correspondence should be addressed to Gwang-Hee Kim; ghkim@kyonggi.ac.kr

Received 1 May 2013; Accepted 8 July 2013

Academic Editor: Alex Li

This research aims to optimize the mixing proportion of recycled aggregate concrete (RAC) using neural networks (NNs) based on genetic algorithms (GAs) for increasing the use of recycled aggregate (RA). NN and GA were used to predict the compressive strength of the concrete at 28 days. And sensitivity analysis of the NN based on GA was used to find the mixing ratio of RAC. The mixing criteria for RAC were determined and the replacement ratio of RAs was identified. This research reveal that the proposed method, which is NN based on GA, is proper for optimizing appropriate mixing proportion of RAC. Also, this method would help the construction engineers to utilize the recycled aggregate and reduce the concrete waste in construction process.

1. Introduction

Recycled aggregate concrete (RAC) has been widely studied in Korea as part of the effort to preserve natural resources and prevent environmental disruption. Currently, many researchers have studied about application of recycled aggregates (RAs) as the base or subbase material in road construction [1] and as a component of high-strength/high-performance concrete [2]. However, RAs have an unavoidable major defect, that is, microcracks and impurities which, occur in the crushing process of original concrete to produce RAs. These microcracks and impurities lead to RAs with higher water absorption, lower specific gravity, and lower durability than natural aggregates (NAs) [3–5]. These RAs have influence on the properties of concrete, such as their workability, shrinkage, tensile strength, compressive strength, and durability in fresh and hardened concrete states.

Therefore, it should be more effective to determine the mixing proportion for RAC than to attempt to improve the quality of the RAs. The quality of concrete, as determined by its compressive strength and durability, depends on the mixing proportions of the concrete and the mixing preparation technique, as well as on the quality of the concrete components [6]. But to date, the mixing proportions of RAC have been determined by experience and knowledge of previous research based on NAs [6]. However, it is inappropriate to determine the mixing proportions of RAC by this way because of the properties of RAs (high water absorption, low specific gravity, and microcracking). Because interrelationships between RAs and the other components of concrete are complex, old cement mortar that does not hydrate on the surface of RAs when attached much, and when using the RAs, this material progresses hydration with reactions with water again. This case, heat of hydration increases because cement amount that reacts actually becomes more than the designed cement amount. Also, a compression, tension, shearing strength, and so forth of RAC should be bigger than normal concrete by augmented cement content theoretically, but actuality is not so, as their interactions are difficult to express by a mathematical (mathematical formula) model [7, 8] and will consume a lot of time. That is, a quantity of all mixing elements should be crystallized again

by an amount of old cement mortar that does not perform hydration reaction when attached on the surface of RAs.

Therefore, it applied a neural network (NN) and a genetic algorithm (GA) to the mixing of RAC as a tool for the solution of those problems. This research proposes criteria for optimal mixing design of a RAC by sensitivity analysis of NN. Also, with designed mixing proportion, it is able to estimate the compressive strength of RAC. Changes in the quality of the RAC according to the mixing ratio of its components were verified by experimental research in the laboratory, and the quality of RAC predicted by the applied NN was compared with the experimental data.

2. Methodology

This research was divided into three main phases (Figure 1). The first step is the processes that make a new data of a variety of kinds for applying to NN-GA model. The second step is the construction of NN model. The third step is applying GA to constructed NN for running of the optimum of NN, and then applying the new data made in first step to the optimized NN. And sensitivity analysis was performed in the constructed NN-GA model.

Generally, the NN is designed for the specific set of input as well as output. The number of inputs and outputs is not restricted, which is one advantage of NN [9, 10]. Then, the number of hidden layer and the number of hidden node are defined. But a large amount of time must be spent in determining them, which is one drawback of NN, because it actually requires some trial-and-error process [11–13]. Therefore, to pare down trifling by repeat of trial-and-error process [14] and to systematic access method [15], the GA was applied to the NN to optimize each parameter of the NN (Figure 1).

3. Experimental Design

3.1. Component Materials. The constituents of the concrete used in this study included ASTM C 150 Type I Portland cement, the specific gravity of which is 3.16, recycled coarse aggregates (RCA), and recycled fine aggregates (RFA), made using first-class aggregates produced from a RAs manufacturing corporation, which is BLUESTONE Corporation in South Korea (water absorption ratios: RFA ≤ 5%, RCA ≤ 3%; specific gravity: RFA ≥ 2.2, RCA ≥ 2.2-KS F 2527, 2574; Korea Standard). The physical properties of the NAs and RAs are shown in Table 1. When it used such RAs because impurities stick much on its surface by production process, compressive strength of RAC decreased [16, 17]. Therefore, in this research, the used RAs were washed in water to remove the effect of impurities on concrete strength. RAs that were wash in water were used after uncover for 48 hours in air.

3.2. Mixing of Concrete. The American Concrete Institute (ACI) Standard 211.1, "Recommended Practice for Selecting Proportions for Normal-Weight Concrete," was used to proportion the concrete mixtures. The RFA was replaced at 0%, 10%, 30%, 50%, 70%, and 100% (by weight), and the RCA was replaced at 0%, 30%, 50%, and 100% (by weight). Table 2 shows a sample of the specified concrete mixing proportions in terms of the replacing ratios for RCA and RFA. The data in Table 2 is used to train the neural networks.

Admixtures, unit water content, unit cement content, and designed compressive strength are as follows:

(i) water/cement ratio (W/C): 50%;

(ii) unit water content: 175 kg/m^3;

(iii) unit cement content: 350 kg/m^3;

(iv) designed compressive strength: 35 MPa.

All test procedures in sieve analysis, specific gravities, and the absorptions of aggregates conformed to ASTM Standards C 136, C 127, and C 128, respectively. Making and curing the concrete and the compressive strength of the cylindrical concrete specimens conformed to ASTM C 192 and ASTM C 39, respectively.

3.3. Casting Test Specimens. Seventy-two casts, for each of which five cylindrical (28-day) concrete specimens were cast (i.e., a total of 360), were prepared for mechanical testing. A cylindrical concrete specimen with a diameter of 100 mm and a depth of 200 mm (ϕ 100 × 200 mm) was used to test the compressive strengths of the samples of RAC. The specimens were casted after the initial curing for 24 hours. Curing was maintained for 28 days in constant temperature and humidity chamber, and the uniaxial compressive test was performed on day 28 by UTM (Universal Testing Machine). The slump of the fresh concrete and the air content were also measured. In Table 2, each data point for slump value and air content rate represents a single test result, and the compressive strength value represents the average value of three test results, after the highest and lowest values among five tests were excluded. To train and test the NN, 216 data sets were used.

3.4. Verifying the Experimental Results. Figure 2 shows a histogram of compressive strength, which is the result of description statistics about experimental data by statistical package for social science. The test results for the cylindrical concrete specimens show a normal distribution, with a mean of 33.75 MPa and a standard deviation of 2.82 MPa. The range of strengths obtained by testing agreed well with the range of the normal distribution curve according to ACI 214-77 [18]. Up to this point in the research, the authors used the mixing proportions for normal concrete as the mixing proportions for the RAC to obtain compressive strength data for the RAC. An average RAC strength was achieved when the mixing proportions of normal concrete with strength of 35 MPa were used for the RAC. To achieve a suitable slump and air content that would allow effective workability of the RAC under the conditions of this experiment, the proper design strength for the RAC should be 33 to 34 MPa. Therefore, as described in Section 4, the range of output values used for the strength estimation and sensitivity analysis of RAC performed in this research was chosen to be 33 to 34 MPa.

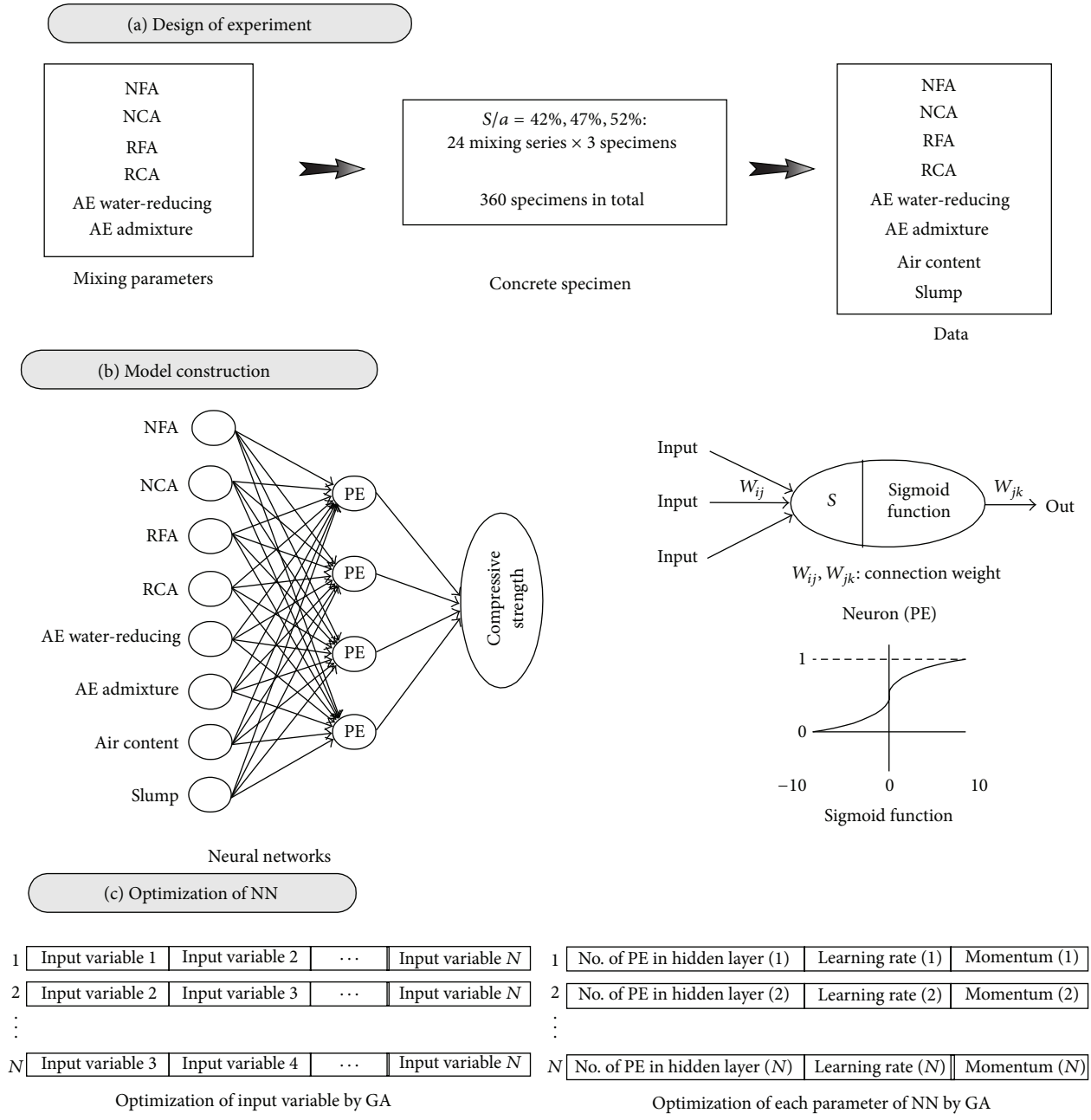

Figure 1: The three steps of this study for RAC mixing. (a) Each factor and *S/a* value of NAs and RAs were used to construct the NN model using how they satisfied the concrete performance criteria (e.g., slump, air content, admixture, and compressive strength), and how they matched the selected factor to receive the factor's optimum value. (b) Each factor's value obtained in "*a*" was applied to the NN input and output variables. The neuron that received the input value displayed the output value using a connection weight. This time and connection weight were calculated using a sigmoid transfer function. (c) The GA was applied to optimize each NN parameter (e.g., momentum, learning rate of the NN, and number of neurons in the hidden layers).

4. Model Construction

In this section, the construction of a compressive strength prediction model based on NN and GA is described. The NN architecture was composed of three layers (Figure 3): input layer, hidden layer, and output layer. The input parameters are seven: NFA, NCA, RFA, RCA, AE water-reducing, AE admixture content, air content, and slump. The output parameter is the compressive strength at day 28. A sample of the cases (24 cases of each S/a: 42%, 47%, and 52%) that were used in the NN training is listed in Table 2.

The learning of NN is accomplished by a backpropagation algorithm (BPN), and the BPN has one of the following transfer functions sigmoid, linear, and exponential functions, that are used to calculate the output for each neuron, except for the input neuron. Among those transfer functions, sigmoid

Table 1: Physical properties of RAs (1st class) and NAs.

Source of aggregate	Fineness modulus	Specific gravity	Water absorption (%)
NCA	6.52	2.64	1.24
NFA	2.52	2.55	1.53
RCA	6.65	2.53	2.86
RFA	3.89	2.43	4.95

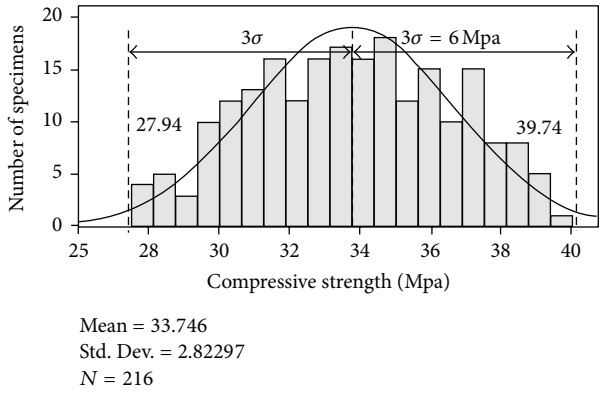

Figure 2: Histogram of compressive strengths of S/a: 42%, 47%, and 52%.

function is used most extensively and has many advantages: (1) has two advantages of linear and exponential functions, (2) is nonlinear function, (3) is differentiable function, and (4) is a S-Pattern. Therefore, the sigmoid function was used as transfer function in this study.

4.1. NN and GA. The NN is inspired by the neuronal structure and operation of the biological brain. Figure 3 shows the simple architecture of backpropagation network with a three-layer network that was used in this study, which consists of an input layer, a hidden layer, an output layer, and the connections between them. The learning mechanism of this backpropagation network is a generalized delta rule, which performs a gradient descent on the error space to minimize the total error between the calculated and desired values of the output layer during modification of the connection weights. The detailed process about backpropagation network is as follows.

(i) At early, NN does connection weights W_{ji} and W_{kj} and biases θ_j and θ_k value to give randomly. Input value N_j and activated value N_j of hidden layer neuron are calculated as a result value O_k for forward by the following equation:

$$N_j = W_{ji} I_i + \theta_j,$$
$$H_i = f\left(N_j\right). \tag{1}$$

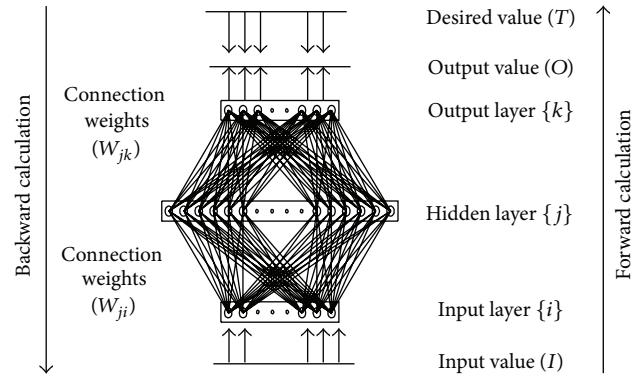

Figure 3: Backpropagation of NN.

Here, $f(x)$ is activation function (sigmoid function), and sigmoid function is represented by the following equation:

$$f(x) = \frac{1}{1 + e^{-(\sum xw - \theta_i)}}. \tag{2}$$

(ii) Delta (δ) is calculated by (3) as difference of target values (D) and result values (O):

$$\delta = (D - O) \times O(I - O). \tag{3}$$

(iii) NN calculates for backward from output layer again. Do a connection weights (W) that is inputted in output layer which is adjusted by the ΔW of the following equation:

$$W_{\text{new}} = W_{\text{old}} + \Delta W,$$
$$\Delta W = \eta \delta H, \tag{4}$$

where η is in the range of between 0 and 1 as invariable of leaning ratio.

(iv) Also, it calculates for backward from hidden layer again. The hidden layer, by the same formula that is calculated for backward in output layer, is calculated toward input layer from the nearest layer to output layer, and the delta of output layer is as follows:

$$\delta = \left(\sum \delta W\right) \times O(I - O). \tag{5}$$

Here, the connection weighting of inputted hidden layer is adjusted by equal method at (iii) step. This backward process is calculated through iteration until it reaches a global minimum point.

(v) Repeat all learning data from (i) to (iv) steps. Uniting MSE (mean squared error) value of all learning data that get by repeating, learning of once is completed

$$\text{MSE} = \frac{1}{2P} \sum_{j=1}^{p} \sum_{i=1}^{n} \left(D_{ij} - O_{ij}\right)^2. \tag{6}$$

In (6), n is the number of hidden layer neurons, and p is the number of learning data.

(vi) If the MSE is not satisfied target error value from (i) step and reached in target error value, this circulation operation is repeated continuously.

Table 2: Sample of specified concrete mixing proportions used for NN training.

S/a (%)	Unit content (kg/m^3)				Admixtures (g)		Air (%)	Slump (cm)	Compressive strength (MPa)		
	NCA	RCA	NFA	RFA	AE-reducing	AE agent					
42	1008.68	0	724.81	0	196	4.9	4.3	21.5	33.71	33.79	33.87
	1008.68	0	652.33	72.48	196	4.9	3.9	22	30.45	28.43	30.43
	706.08	302.60	507.37	217.44	196	2.45	5.8	22	33.64	32.65	33.74
	706.08	302.60	362.405	361.405	196	2.45	2.0	23	35.79	32.80	37.02
	504.34	504.34	362.405	361.405	196	2.45	2.8	25	33.71	36.13	34.38
	504.34	504.34	0	724.81	196	2.45	2.3	20	31.67	31.68	26.35
	0	1008.68	724.81	0	196	2.45	4.5	17	32.22	28.39	28.58
	0	1008.68	652.33	72.48	196	2.45	4.5	20	30.42	28.90	32.34
47	921.73	0	567.77	229.19	196	1.225	6.0	22.5	35.83	36.01	35.44
	921.73	0	405.55	381.97	196	1.225	3.3	10	38.16	38.23	36.16
	645.21	270.14	729.99	76.39	196	1.225	5.6	11	34.91	35.30	33.52
	645.21	270.14	567.77	229.19	196	1.225	4.7	17	35.94	35.03	34.66
	460.86	450.23	567.77	229.19	196	1.225	3.8	22.5	33.70	29.98	35.30
	460.86	450.23	405.55	381.97	196	1.225	3.3	19	32.35	35.48	35.23
	0	900.46	243.33	534.76	196	1.225	2.5	21	34.15	34.11	34.92
	0	900.46	0	763.94	196	1.225	3.5	17	30.52	31.34	33.15
52	834.77	0	807.64	84.52	196	0	7.2	22.5	29.08	30.27	29.99
	834.77	0	628.17	253.26	196	0	6.8	23	27.64	29.29	30.61
	584.34	244.65	897.38	0	196	0	2.1	25	30.65	33.06	34.66
	584.34	244.65	448.69	422.6	196	0	2.8	21	32.87	30.62	29.82
	417.39	407.75	807.64	84.52	196	0	3.4	16.5	32.78	33.13	31.87
	417.39	407.75	628.17	253.26	196	0	3.4	16	33.09	34.03	33.48
	0	815.51	897.38	0	196	0	3.0	14.5	35.60	31.52	32.64
	0	815.51	807.64	84.52	196	0	3.4	15	35.63	29.06	29.97

The GA employs Darwinian selection and Mendelian crossover principles. Because GAs are robust and guided random search methods, they have found a niche in the nonlinear programming field. GA is based on the collective learning of a population, the individuals of which represent the potential solutions for the problem to be solved. GA transfers a group of genetic individuals from one generation to the next. A set of individuals from the same generation is known as a population. Each population goes through a series of genetic operators, that is, selection, recombination, or variation, to produce the next generation. An in-depth analysis is given in [19].

NN is commonly used for difficult tasks involving intuitive judgment or requiring the detection of data patterns that elude conventional analytic techniques. The performance of NN, however, is affected by the network architecture and its parameter settings. In NN models, these factors have been determined by heuristic and trial-and-error methods, which are time-consuming and tedious [14]. Therefore, in this research, a primary role of the GA is to determine the number of neurons in the hidden layers, the momentum, the learning rate of the NN and to select the appropriate input variables. Application method of GA to search for a combination of input variables of NN for optimum performance of NN model is as follows.

(i) If the number of input variables is "n," GA composes individual by random such as in Figure 1(c) with input variable of "n." This time, number of individual is created as population size (N) of GA.

(ii) Each individual corresponded with input variable of NN, and corresponded input variable is applied to NN and the NN learn. The learned MSE of NN gets fitness value of each chromosome.

(iii) Individuals which the fitness valued pass hybridization (crossover) or mutation process. At this process, individuals that have excellent fitness value exist, and individuals that are not so disappear.

(iv) Until reaching optimum result, process of (ii) and (iii) as established number of households is repeated. Passing through this process, chromosomes that have a bad influence upon result value of NN disappears, and individuals whose fitness is superior exist. As this, combination of input variable whose estimation correctness of NN is high is decided. A more in-depth content is given in [20].

4.2. Implementation of NN and GA. The GA application process for optimizing the number of input variables in the input layer, the number of neurons in the hidden layer, and

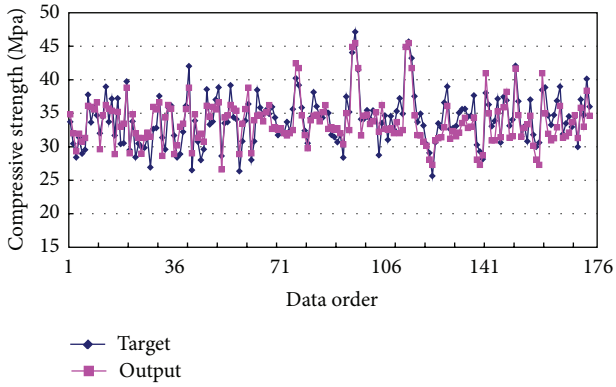

Figure 4: Results of training with 176 data sets.

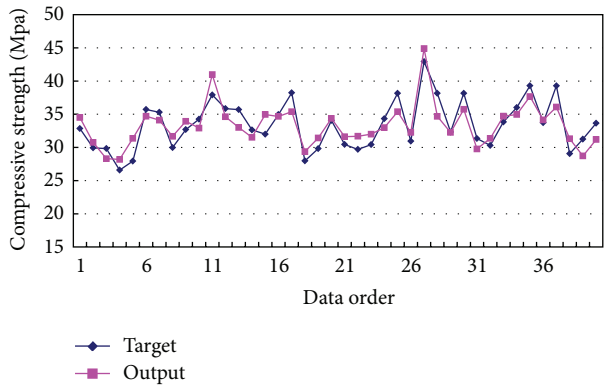

Figure 5: Results of testing the trained model (40 data sets).

the coefficient of learning rates of NN was as follows. First, the numbers of hidden layers and output neurons in the NN were set to 1 (2 and 3) and 1, respectively. All chromosomes were automatically set in NN so that they consisted of the numbers of input variables, of hidden neurons, and of learning rates. NN also automatically produced their initial values. The values for these input variables were set in a range with a lower limit of X and an upper limit of nX (where X is an input variable and n is the number of input variables). The hidden neuron number was set in a range with a lower limit of 0.75 m and an upper limit of $2m+1$ (where m is the number of hidden neurons). The step size had a lower limit of 0 and an upper limit of 1, and the momentum had a lower limit of 0 and an upper limit of 1. The numbers of chromosomes (population size) and generations were set to 100 and 50, respectively.

After the parameter values (number of input variables, hidden neurons, step size, and momentum for each chromosome) were translated into the predefined NN, the network of NN was trained on the training data set. A cross-validation data set was used to test whether the stopping criteria were satisfied. The training process for the BPN stopped after a maximum of 1,000 epochs or until there was no improvement in mean squared error (MSE) for 1,000 epochs on the cross-validation data set. The fitness of every chromosome was evaluated by measuring the MSE, which is the estimated result on a cross-validation data set.

The number of data sets used to train the NN was 176, and the average training error was 5.26% (lowest training error 0.06%, highest training error 9.94%). As can be seen in Figure 4, the model was successfully trained. The model gave values that were very close to the actual values and was able to follow the trend of the actual values. On the other hand, the extreme values of the targeted compressive strengths could not be obtained from the model because the model was conservative, and it required more extreme training data to learn the extremes.

The test results given in Figure 5 are compared with the 40 actually measured data sets tested in the trained model. As can be seen in Figure 5, the performance of the model was very good, with an average error of 5.10% (lowest 0.21% and highest 9.23%).

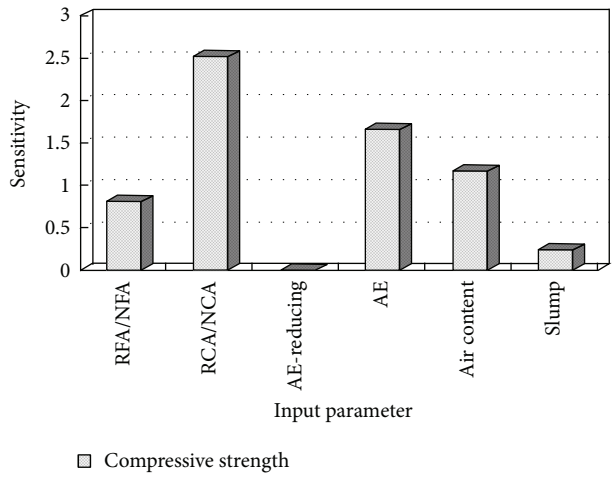

Figure 6: Sensitivity about the mean showing the dependence on the input parameters.

4.3. Sensitivity Analysis. The sensitivity of the input variables of the NN (such as RCA, RFA, and air content) to the compressive strength of the RAC was also analysed using the constructed NN model.

Because properties of RAs are different from those of NAs, shape, surface, impurity content, agent usage, and others, it is required to research how much those properties of NAs have an effect on the compressive strength of RAC. And based on the sensitivity analysis, a mixing design of RAC will be made. Sensitivity analysis evaluates the changes in training error resulting from a change in an input value. The 216 data points obtained by experimentation were used to analyse the sensitivity of the input variables. In this study, NN with 2 hidden layers optimized by GA was used for the sensitivity analysis and to map the inputs and outputs.

5. Result and Discussion

The sensitivity of RCA/NCA, which represents the change in compressive strength according to the replacement ratio of

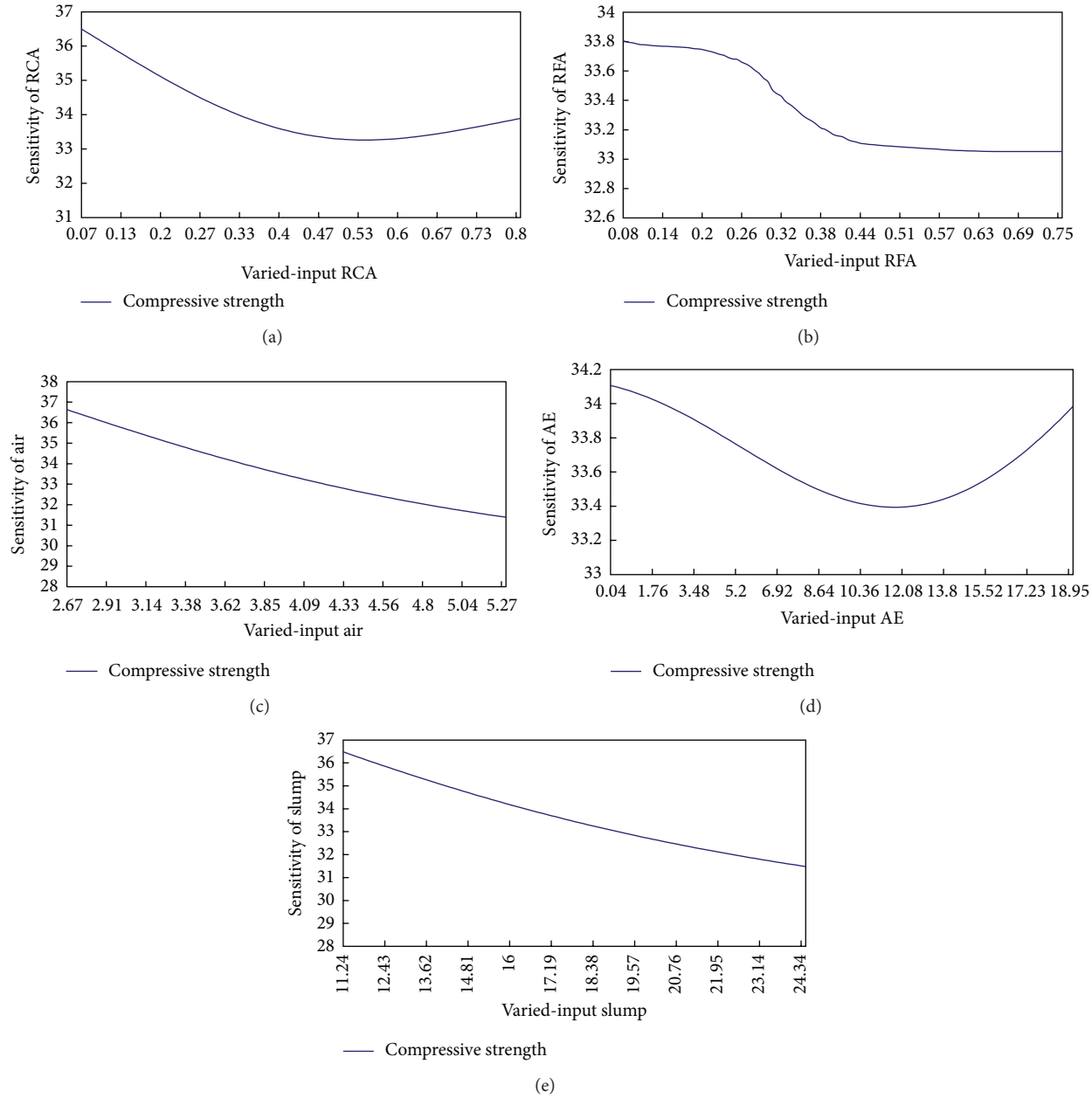

Figure 7: Sensitivity of the input parameters to the compressive strength, showing the effect of varying the input value on the parameters.

RCA, shows a relatively higher value in Figures 6 and 7 than other input parameters because RCA is angular and rough. On the other hand, because the surface area of the bond between an aggregate and cement paste increases or decreases according to changes in the replacement ratio of RCA, the concrete strength can vary sharply. The mixing ratio of RCA affects the compressive strength of RAC.

In Figure 6, the replacement ratio of RFA shows a lower sensitivity value than the replacement ratio for RCA relative to the compressive strength of RAC. And in Figure 7, the compressive strength of RAC decreases with increases in the replacement ratio of RFA. In particular, the compressive strength appears to decrease rapidly between the inputs RFA values of 0.26 and 0.44. In this case, some water may be absorbed by the RA; the more aggregate, the more water is absorbed. However, an aggregate content above a certain amount would lead to less shrinkage and less bleeding, and therefore, to less damage in the bond between the aggregate and the cement paste [21]. Therefore, whereas the compressive strength was abruptly lost between 0.26 and 0.44, the compressive strength did not change when the RFA value was greater than 0.44.

In Figure 7, the output value decreased to 12.08 with increases in AE, and then increased again. This result shows

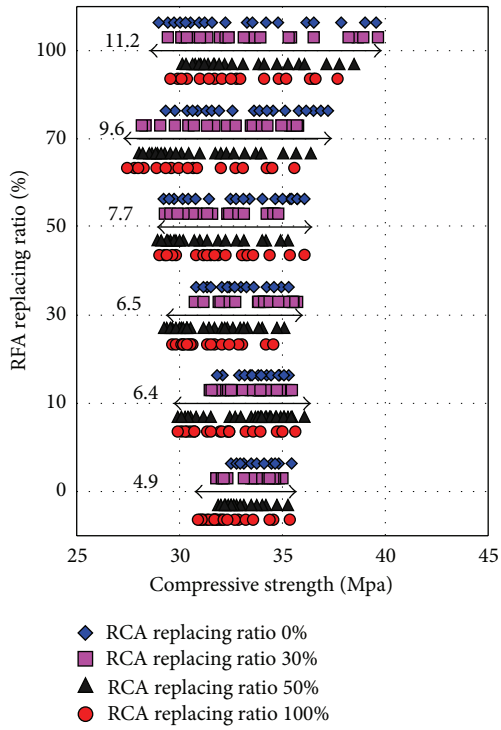

Figure 8: Deflection of compressive strength with RCA and RFA replacing ratios.

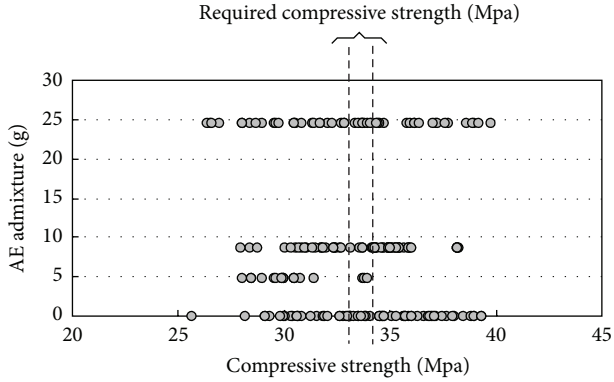

Figure 9: Range of AE admixture.

that the AE admixture acts in RAC in the same way as in normal concrete: when air voids are incorporated into the cement paste matrix, either as a result of inadequate compaction or through the use of an AE admixture, they also increase the porosity and decrease the strength of the system. The graph of "output × variable input air" shows that the concrete suffered considerable loss of strength with increasing amounts of entrained air.

Sensitivity analysis shows that compressive strength was more affected by the replacement ratio of RCA than by the replacement ratio of RFA. The deflection of compressive strength by the cross-matches of RCA and RFA is shown in Figure 8. The deflection of compressive strength of RAC becomes more significant as the replacement ratio of RCA

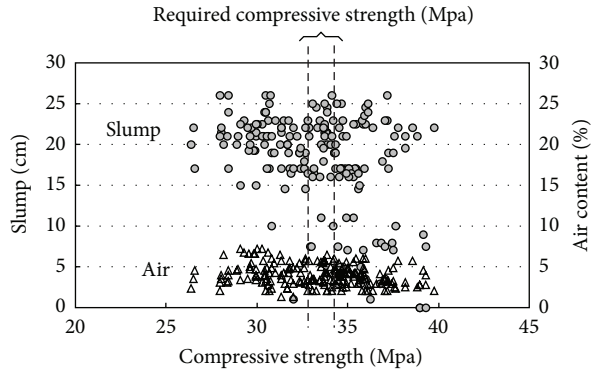

Figure 10: Range of slump and air content.

increases. Note that the deflection became very serious when the replacement ratio of RCA exceeded 50%; with increasing the replacement ratio of RAs, it means that it is difficult to acquire concrete of designed compressive strength. The effects of AE admixture on compressive strength are shown in Figure 9. Under the conditions of this experiment (W/C: 50%; unit water content: 175 kg/m^3; unit cement content: 350 kg/m^3; acquired compressive strength: 33 to 34 MPa; and S/a: 42%, 47%, and 52%), the compressive strength of RAC did not change when the amount of AE admixture added to the RAC was between 5 g and 10 g. However, when the amount of AE admixture was under 5 g and over 10 g, the compressive strength of the RCA deviated considerably from the average value. Therefore, the AE admixture must be used carefully with the RAC. Slump and air content influence the workability and strength of concrete, although air is used to make concrete resistant to freezing and thawing. The compressive strength of concrete is important, but other properties that are relevant when it is being transported, possibly pumped, and placed, are equally important. The suitable range of slump values and air contents for each is 20 ± 1.5 and 4.5 ± 0.5, respectively (Figure 10).

It acquired criteria (Table 3) for optimum mixing of RAC that have compressive strength 33~34MPa by this research until now. And it makes the RAC confirm whether these criteria are suitable or were not so and measure a slump, an air content, and a compressive strength at 28 days.

The replacement ratio of RAs applied the maximum value (RCA 30% and RFA 50% at S/a 42%; RCA 50% and RFA 50% at S/a 47%; RCA 50% and RFA 30% at S/a 52%) that is registered in Table 3 considering the worst situation, and a W/C did the 50%. There is the result in Table 4. Air and a slump values among the test values were included in a range of the target value, and average compressive strength of three specimens was lower than the target values except an S/a 42%. But the test values were within the target value in general.

6. Conclusion

This study presents an appropriate quality range for RAs and the other components of RAC using sensitivity analysis with neural networks, for use in the production of RAs and

Table 3: Summary of results (approximate range of each parameter).

Required strength (MPa)	S/a (%)	Air (%)	Slump (cm)	Replacement ratio (%)		Admixtures (g)	
				RCA (1st Class)	RFA (1st Class)	AE-water reducing agent	AE agent
33~34	42	4.5 ± 0.5	20 ± 1.5	0~30%	0~50%	196	5~10
	47			0~50%	0~50%	196	5~10
	52			0~50%	0~30%	196	—

Table 4: Criteria evaluation.

S/a (%)	Unit content (kg/m^3)						Admixtures (g)		Target value			Test value		
	Cement	Water	NCA	RCA	NFA	RFA	AE-water reducing agent	AE agent	Air (%)	Slump (cm)	Strength (MPa)	Air (%)	Slump (cm)	Strength (MPa)
42	350	175	719.7	291	368.9	350.2	202	4.9	4.5 ± 0.5	20 ± 1.5	33	4.2	18.4	34.4
47			469.7	443.1	412.9	391.9	205	1.225				4.1	21.7	31.7
52			425.4	401.3	632.9	257.5	203	1.014				4.2	20.1	31.5

RAC, and ultimately to promote the use of RAs in concrete. In this study, the mixing criteria of the basic concrete for RAC were determined. RCA content and the AE admixture content are the most important to the compressive strength of RAC. Finally, the results of this study will be applied to use in various mixing proportions of recycled concrete. This research will contribute to improve the usage of the recycled aggregate in construction industry and to reduce the waste in construction process.

References

[1] T. Bennert, J. Papp W.J., A. Maher, and N. Gucunski, "Utilization of construction and demolition debris under traffic-type loading in base and subbase applications," *Transportation Research Record*, no. 1714, pp. 33–39, 2000.

[2] A. Ajdukiewiez and A. Kliszezewiez, "Influence of recycled aggregates on mechanical characteristics of HS/HPS," *Cement and Concrete Research*, vol. 24, no. 2, pp. 269–279, 2002.

[3] Y. H. Lin, Y. Y. Tyan, T. P. Chang, and C. Y. Chang, "An assessment of optimal mixture for concrete made with recycled concrete aggregates," *Cement and Concrete Research*, vol. 34, no. 8, pp. 1373–1380, 2004.

[4] R. Zaharieva, F. Buyle-Bodin, and E. Wirquin, "Frost resistance of recycled aggregate concrete," *Cement and Concrete Research*, vol. 34, no. 10, pp. 1927–1932, 2004.

[5] R. M. Salem, E. G. Burdette, and N. M. Jackson, "Resistance to freezing and thawing of recycled aggregate concrete," *ACI Materials Journal*, vol. 100, no. 3, pp. 216–221, 2003.

[6] K. H. Yang and K. H. Lee, "Tests on alkali-activated slag foamed concrete with various water-binder ratios and substitution levels of fly ash," *Journal of Building Construction and Planning Research*, vol. 1, no. 1, pp. 8–14, 2013.

[7] J. W. Oh, I. W. Lee, J. T. Kim, and G. W. Lee, "Application of neural networks for proportioning of concrete mixes," *ACI Materials Journal*, vol. 96, no. 1, pp. 61–67, 1999.

[8] N. Al-Mutairi, M. Terro, and A. Al-Khaleefi, "Effect of recycling hospital ash on the compressive properties of concrete: statistical assessment and predicting model," *Building and Environment*, vol. 39, no. 5, pp. 557–566, 2004.

[9] G. H. Kim, J. M. Shin, S. Kim, and Y. Shin, "Comparison of school building construction costs estimation methods using regression analysis, neural network, and support vector machine," *Journal of Building Construction and Planning Research*, vol. 1, no. 1, pp. 1–7, 2013.

[10] J. M. de la Garza and K. G. Rouhana, "Neural networks versus parameter-based applications in cost estimating," *Cost Engineering*, vol. 37, no. 2, pp. 14–18, 1995.

[11] A. E. Smith and A. K. Mason, "Cost estimation predictive modeling: regression versus neural network," *Engineering Economist*, vol. 42, no. 2, pp. 137–161, 1997.

[12] S. Kim, "Hybrid forecasting system based on case-based reasoning and analytic hierarchy process for cost estimation," *Journal of Civil Engineering and Management*, vol. 19, no. 1, pp. 86–96, 2013.

[13] H. Li, "Neural networks for construction cost estimation," *Building Research and Information*, vol. 23, no. 5, pp. 279–284, 1995.

[14] T. Hegazy, P. Fazio, and O. Moselhi, "Developing practical neural network applications using back-propagation," *Microcomputers in Civil Engineering*, vol. 9, no. 2, pp. 145–159, 1994.

[15] E. Vonk, L. C. Jain, and R. P. Johnson, *Automatic Generation of Neural Network Architecture Using Evolutionary Computation*, World Scientific, Singapore, 1999.

[16] A. Katz, "Properties of concrete made with recycled aggregate from partially hydrated old concrete," *Cement and Concrete Research*, vol. 33, no. 5, pp. 703–711, 2003.

[17] H. Chen, T. Yen, and K. Chen, "Use of building rubbles as recycled aggregates," *Cement and Concrete Research*, vol. 33, no. 1, pp. 125–132, 2003.

[18] "ACI 214-77 (Reapproved 1989). Recommended practice for evaluation of strength test results of concrete, ACI Manual of concrete Practice, Part 2: construction Practices and Inspection Pavement," Detroit, Michigan, 1994.

[19] T. Munakata, *Fundamentals of the New Artificial Intelligence: Beyond Traditional Paradigms*, Springer, New York, NY, USA, 1998.

[20] G. H. Kim, J. E. Yoon, S. H. An, H. H. Cho, and K. I. Kang, "Neural network model incorporating a genetic algorithm in estimating construction costs," *Building and Environment*, vol. 39, no. 11, pp. 1333–1340, 2004.

[21] O. Pastor-Bárcenas, E. Soria-Olivas, J. D. Martín-Guerrero, G. Camps-Valls, J. L. Carrasco-Rodríguez, and S. Del Valle-Tascón, "Unbiased sensitivity analysis and pruning techniques in neural networks for surface ozone modelling," *Ecological Modelling*, vol. 182, no. 2, pp. 149–158, 2005.

Hindawi Publishing Corporation
Advances in Materials Science and Engineering
Volume 2013, Article ID 918294, 5 pages
http://dx.doi.org/10.1155/2013/918294

Research Article

Effect of Ground Waste Concrete Powder on Cement Properties

Xianwei Ma[1] and Zhenyu Wang[2]

[1] *Department of Civil and Material Engineering, Henan University of Urban Construction, Pingdingshan 467036, China*
[2] *College of Civil Engineering and Architecture, Zhejiang University, Hangzhou 310058, China*

Correspondence should be addressed to Zhenyu Wang; wzyu@zju.edu.cn

Received 20 March 2013; Revised 1 May 2013; Accepted 13 May 2013

Academic Editor: Alex Li

The paste/mortar attached to the recycled aggregate decreases the quality of the aggregate and needs to be stripped. The stripped paste/mortar is roughly 20% to 50% in waste concrete, but relevant research is very limited. In this paper, the effects of ground waste concrete (GWC) powder, coming from the attached paste/mortar, on water demand for normal consistency, setting time, fluidity, and compressive strength of cement were analyzed. The results show that the 20% of GWC powder (by the mass of binder) has little effect on the above properties and can prepare C20 concrete; when the sand made by waste red clay brick (WRB) replaces 20% of river sand, the strength of the concrete is increased by 17% compared with that without WRB sand.

1. Introduction

With the rapid development of urbanization, many old buildings have been demolished and a lot of construction waste is generated. In China, construction waste produced from building demolition is estimated to be 400 million tons per year. Landfilling is the most common treatment method, but it leads to the special problem of environment pollution. In addition, the location suitable for landfill is increasingly difficult to find so that the fee of landfill becomes higher. The recycling of construction waste, therefore, is encouraged and supported in many counties.

In China, mostly old buildings of 20 years ago belong to the brick-concrete structure and construction waste includes about 20–30% waste concrete, 30–40% red clay brick, and 5%–10% other waste such as glass and ceramic tile. Extensive research has been conducted, but many are related to the recycling use of waste concrete aggregates [1–7]. When waste concrete is crushed, a certain amount of cement paste/mortar is attached to the surface of aggregates. The attached paste/mortar is the main reason for the lower quality of the recycled aggregate compared with the natural aggregate. The concrete with the recycled aggregate generally has inferior strength and durability. Some aggregate refining methods such as "heating and rubbing" [8] and "mechanical grinding" [9] have been developed in order to improve the quality of recycled aggregates by removing the attached paste/mortar. The amount of paste/mortar in waste concrete is about between 20% and 50%, but relative research is very limited [10–13]. Lv found that when waste concrete powder content is lower than 30%, its effect on cement strength is the same as fly ash's and that its effect becomes more evident after heat treatment [11].

In order to effectively utilize waste concrete, the effects of ground waste concrete (GWC) powder on water demand for normal consistency, setting time, fluidity, and compressive strength of cement were analyzed and the feasibility of C20 concrete prepared with recycled aggregate and GWC powder was also discussed in this paper.

2. Materials and Methods

2.1. Materials. The GWC powder was obtained by crushing and grinding the tested OPC concrete specimens in the laboratory. Figure 1 shows the composition of the GWC powder based on XRD analysis. The constituents of the GWC powder are quartz, $Ca(OH)_2$, mullite (from fly ash in cement), tobermorite, and a small amount of unhydrated C_2S. Tobermorite is formed by the crystallization of C-S-H gel.

PF32.5 grade fly ash cement was adopted and its properties met the requirements of common Portland cement (GB175-2007).

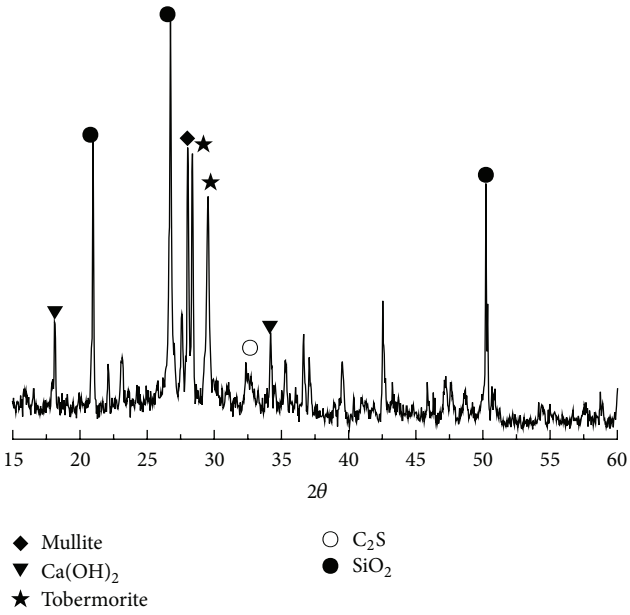

Figure 1: XRD pattern of GWC powder.

River sand met the requirements of the sand used in construction (GB/T-14684-2011).

2.2. Experimental Methods. After the 28 days, cured concrete specimens had been tested and left in the air for another 3 months; they were crushed by a jaw crusher and separated into different parts based on particle size. The part passing through the 0.3 mm sieve was subject to further grinding using a grinding mill so as to ensure that most particles pass through the 0.075 mm sieve. The obtained GWC powder was mixed with cement at different proportions, 0%, 10%, 20%, 30%, and 40% (by the mass of binder). Water demand for normal consistency, setting time, fluidity, and compressive strength of cement were tested according to the requirement of GB175-2007 common Portland cement.

3. Results and Discussions

3.1. Water Demand for Normal Consistency and Setting Time of Cement Paste. Table 1 gives water demand for normal consistency (WDNC) and setting time of cement pastes with different amounts of GWC powder. The amount of binding material was 500 g.

With increasing the amount of GWC powder, WDNC is decreased. When the amount of GWC powder is more than 30%, WDNC is evidently reduced. For example, WDNC of a sample with 40% of GWC powder drops by 9%. The reason is that GWC powders contain a small amount of unhydrated C_2S (Figure 1) which slowly reacts with water, and other minerals do not react with water. As a result, WDNC is mainly related to the amount of cement in the GWC-cement system. The reduction of cement's amount in the sample naturally leads to the decrease of WDNC. In addition, Wu et al. analyzed the effect of different fitness of GWC powder on WDNC and found that the increase of the fitness has a much lower effect on WDNC [13].

The GWC powder, however, has almost no effect on setting time of cement.

Table 1: WDNC and setting time of cement with different amounts of the GWC powder.

GWC powder amount/%	The depth of the cone falling/mm	WDNC/g	Initial set/min	Final set/min
0	28	150	111	228
10	27	147	109	232
20	28	143	113	237
30	29	140	108	233
40	28	137	110	230

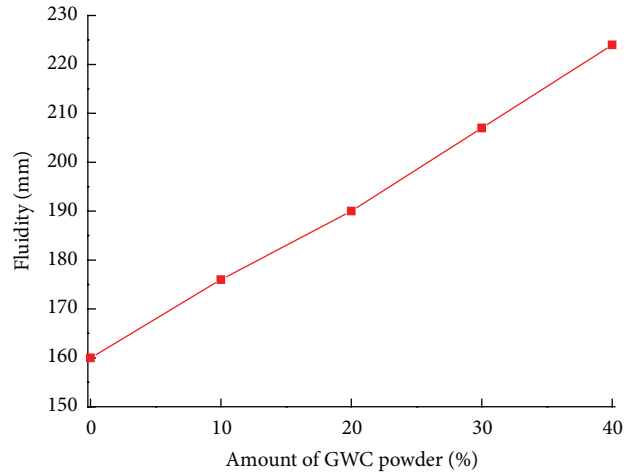

Figure 2: Change in fluidity of mortar with GWC powder amount.

3.2. Fluidity of Cement Mortar. The water/binder ratio of cement mortar remained 0.5. The fluidity of cement mortar with different amounts of GWC powder is shown in Figure 2. The fluidity is almost lineally raised with GWC powder amount rising. For the samples with 40% of GWC powder, for instance, the fluidity is increased by about 40%.

The change in the fluidity is consistent with that of WDNC, but it does not agree with the results of Lv et al. that the GWC powder decreased the fluidity [11]. Lv et al. thought that the surface of ground particles has some pores which absorb some water. However, the main reason may be the different amount of active particles which react with water and lead to the decrease of free water amount. GWC powder, in our experiment, only contains a very small amount of C_2S which has a very slow rate and can be thought not to be active.

3.3. The Strength of Hardened Cement Mortar. Compressive and flexural strengths of hardened cement mortar with different amounts of GWC powder are shown in Figures 3 and 4. Compressive strengths at 3 and 28 days are reduced with GWC powder amount rising. When the amount of GWC powder is less than 20%, the downward trend of the

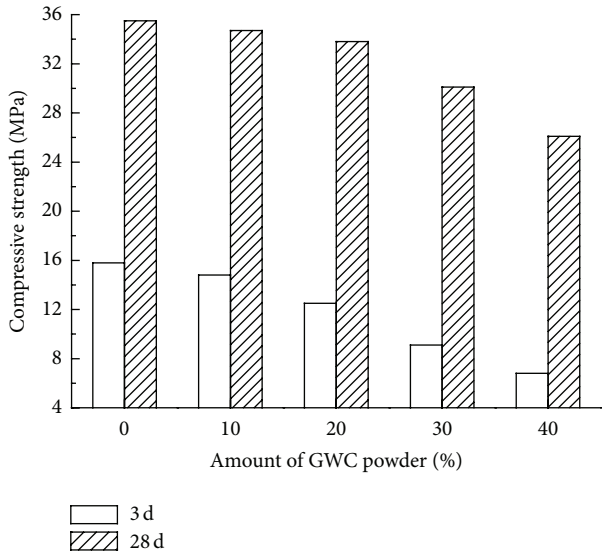

Figure 3: Compressive strength of mortar with different amounts of GWC powder.

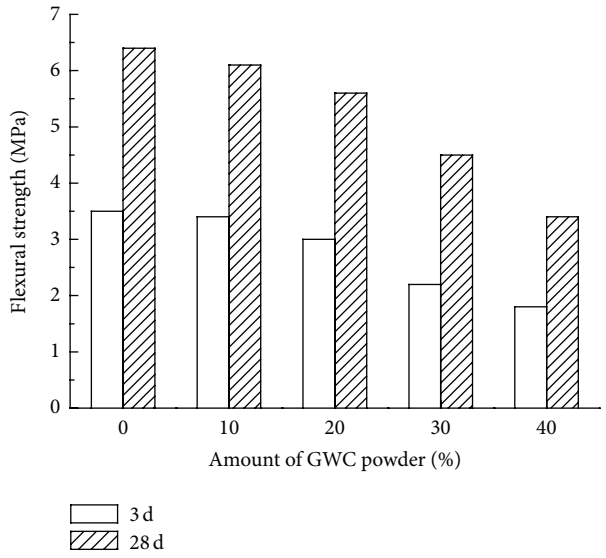

Figure 4: Flexural strength of mortar with different amounts of GWC powder.

strength is not very obvious. However, more than 20% of GWC powder evidently decreases the strength. For example, the strength of the sample with 40% of GWC powder falls by 57% at 3 days and by 26% at 28 days. The change in flexural strength with GWC powder amount is similar to that of compressive strength.

The above results indicate that the inference in Section 3.2 is correct; namely, the hydration activity of the GWC powder is lower. In fact, the building demolished in China was built about 20 years ago and cement in waste concrete had almost been completely hydrated.

For the active excitation of GWC powder, a common method is heat treatment in the range of temperature, such

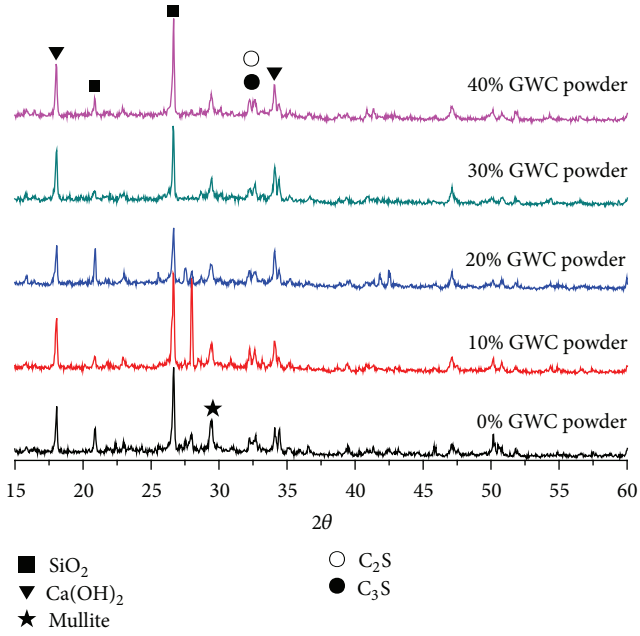

Figure 5: XRD pattern of hardened paste.

as 500–800°C. After heating, some active minerals are formed and improve the strength [11, 12]. However, the heat treatment for GWC powder is difficult to be realized in the ordinary building material companies. The active effect of GWC powder, therefore, is not to be further researched in this paper.

It needs to be noticed that the 20% of GWC powder has little effects on compressive strength (falling only 1.5 MPa) and would bring considerable economic benefit. The following design relating to the recycled concrete is based on the 20% of replacement.

3.4. Constituents and Structures of Hardened Paste. An XRD pattern of hardened paste with the GWC powder at 28 days is shown in Figure 5. The major constituents of the hardened paste are SiO_2, $Ca(OH)_2$, mullite, C-S-H, and a small amount of unhydrated C_2S and C_3S. SiO_2 is provided by the GWC powder. The intensities of unhydrated C_2S and C_3S (about 32.5°) in all the samples are almost the same but the intensities of the SiO_2 peak (about 26°) do not change with the amount of the GWC powder. The results indicate that the amount of each mineral in the GWC powder is very unsteady, but the selecting and treating procedures of sample are very different to control. Luckily, the amount of unhydrated cement in the GWC powder is very low and has little contribution to the cementitiousness of hardened paste so that the change of strength caused by the amount of the GWC powder still shows a relatively reasonable trend.

The morphology of hardened paste with the GWC powder at 3 and 28 days is shown in Figure 6. Amorphous C-S-H gel, needle-like Aft, and blocky $Ca(OH)_2$ are easily found in the 3 days' samples. The main difference is that, at 3 days, the structure of the sample with the GWC powder is looser than

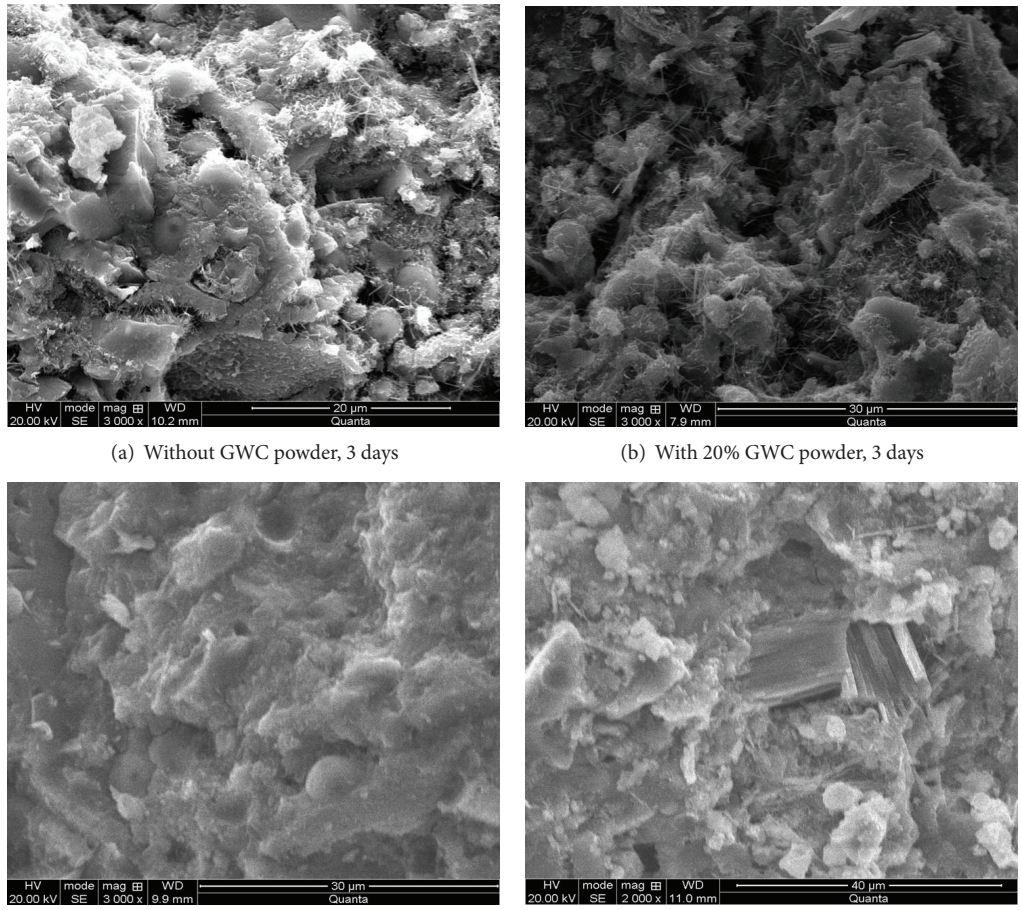

(a) Without GWC powder, 3 days

(b) With 20% GWC powder, 3 days

(c) Without GWC powder, 28 days

(d) With 20% GWC powder, 28 days

Figure 6: Morphology of hardened paste.

that without the GWC powder, but the difference becomes unobvious at 28 days. The results indicate that the 28 days' strength should not vary much in both samples (actually 1.5 MPa).

3.5. C20 Recycling Concrete Design. The replacement of 32.5 grade fly ash cement by the GWC powder was 20%. Recycled aggregate came from waste concrete in the laboratory. Recycled sand made by waste red clay bricks (WRB) was used to replace river sand, and WRB sand had the same particle size distribution and fineness module as river sand. The ratio of cement, stone, sand, and water was 1 : 1.95 : 3.05 : 0.56.

Table 2 gives compressive strength and slump of concrete with WRB sand. Without WRB sand, the strength has reached 23.6 MPa at 28 days. When WRB sand is added, the slump is reduced but the strength is increased. For example, when WRB sand replaces 20% of river sand, the strength is increased by 17% compared with that without WRB sand. The results may be related to the porous structure of WRC sand which absorbs some water in mixing and releases the water during the hardening. The released water will promote the hydration of cement. Wang and Xiao et al. also found the reinforcement of WBC as aggregate [14, 15].

The aforementioned results indicate that WRB sand is a very promising concrete additive and should be further researched. Relevant research would be of considerable benefit and promote the effective utilization of construction waste.

Table 2: Compressive strength and slump of concrete with WRB sand.

SRCB amount/%	Compressive strength/MPa		Slump/mm
	3 d	28 d	
0%	7.5	23.6	45
10%	7.8	25.8	40
20%	9.0	27.7	30

4. Conclusions

(1) The GWC powder decreases water demand for normal consistency (WDNC) of cement paste, especially when the amount of the GWC powder is more than 30%, but it has almost no effect on setting time.

(2) When the water/binder of cement mortar is 0.5, the fluidity is almost lineally raised with GWC powder amount.

(3) When the amount of the GWC powder is less than 20%, the downward trend of the strength is not very

obvious. More than 20% GWC powder, however, evidently decreases the strength.

(4) Compressive strength of concrete with 20% GWC powder and recycled aggregate reaches 23.6 MPa at 28 days. When WRB sand replaces 20% of river sand, the strength is increased by 17% compared with that without WRB sand.

Acknowledgment

This work is supported by the Research Foundation of Henan University of Urban Construction (no. 2012JZD001).

References

[1] T. C. Hansen, *Recycling of Demolished Concrete and Masonry*, Taylor and Francis, Oxford, UK, 1992.

[2] M. Tavakoli and P. Soroushian, "Strengths of recycled aggregate concrete made using field-demolished concrete as aggregate," *ACI Materials Journal*, vol. 93, no. 2, pp. 182–190, 1996.

[3] K. K. Sagoe-Crentsil, T. Brown, and A. H. Taylor, "Performance of concrete made with commercially produced coarse recycled concrete aggregate," *Cement and Concrete Research*, vol. 31, no. 5, pp. 707–712, 2001.

[4] A. Shayan and A. Xu, "Performance and properties of structural concrete made with recycled concrete aggregate," *ACI Materials Journal*, vol. 100, no. 5, pp. 371–380, 2003.

[5] V. W. Y. Tam, X. F. Gao, and C. M. Tam, "Microstructural analysis of recycled aggregate concrete produced from two-stage mixing approach," *Cement and Concrete Research*, vol. 35, no. 6, pp. 1195–1203, 2005.

[6] J. Z. Xiao, J. B. Li, and C. Zhang, "On relationships between the mechanical properties of recycled aggregate concrete: an overview," *Material Structure*, vol. 39, pp. 655–364, 2006.

[7] M. Malešev, V. Radonjanin, and S. Marinković, "Recycled concrete as aggregate for structural concrete production," *Sustainability*, vol. 2, pp. 1204–1225, 2010.

[8] C. Thomas, J. Setién, J. A. Polanco, P. Alaejos, and M. Sánchez de Juan, "Durability of recycled aggregate concrete," *Construction and Building Materials*, vol. 40, pp. 1054–1065, 2013.

[9] K. Yasuhiro, H. Hiroshi, U. Noboru, N. Yoko, Y. Nobuyuki, and M. Yoshiaki, "A closed-loop concrete system on a construction site," *Technical Research Report of Shimizu Corporation*, vol. 79, pp. 1–10, 2004.

[10] Y. Kunio, I. Kazumasa, S. Shigeki, and T. Daijiro, "A study of cyclic use of aggregate for structural concrete," *Takenaka Technical Research Report*, no. 62, pp. 5–16, 2006.

[11] X. Y. Lv, L. S. Wang, X. Chen, and Q. Y. Li, "Experimental study on the activity of concrete recycled powder," *Journal of Qingdao Technological University*, vol. 30, pp. 137–139, 2009.

[12] S. G. Hu and Y. J. He, "Preparation of regenerated binding materials using waste concrete," *Journal of the Chinese Ceramic Society*, vol. 35, pp. 593–598, 2007.

[13] X. M. Wu, J. J. Yang, and M. Huang, "Construction waste ground powder as mineral admixtures on the influence of the physical and mechanical properties of cement," *New Building Materials*, no. 4, pp. 16–17, 2004.

[14] W. X. Wang, "Performance of concrete with renewable waste brick aggregate modified by fly ash," *Building Block and Block Construction*, no. 1, pp. 12–14, 2007.

[15] B. Xiao, Z. Z. Liu, X. L. Li et al., "Experimental study on recycling waste bricks as aggregates," *Journal of Taizhou University*, vol. 32, no. 6, pp. 51–55, 2010.

Hindawi Publishing Corporation
Advances in Materials Science and Engineering
Volume 2013, Article ID 478421, 7 pages
http://dx.doi.org/10.1155/2013/478421

Research Article

Behavior of HPC with Fly Ash after Elevated Temperature

Huai-Shuai Shang[1,2] and Ting-Hua Yi[3]

[1] *School of Civil Engineering, Qingdao Technological University, Qingdao 266033, China*
[2] *State Key Laboratory of Structural Analysis for Industrial Equipment, Dalian University of Technology, Dalian 116024, China*
[3] *Faculty of Infrastructure Engineering, Dalian University of Technology, Dalian 116023, China*

Correspondence should be addressed to Huai-Shuai Shang; shanghuaishuai@yahoo.com.cn

Received 3 January 2013; Accepted 10 March 2013

Academic Editor: Dimitar Dontchev

For use in fire resistance calculations, the relevant thermal properties of high-performance concrete (HPC) with fly ash were determined through an experimental study. These properties included compressive strength, cubic compressive strength, cleavage strength, flexural strength, and the ultrasonic velocity at various temperatures (20, 100, 200, 300, 400 and 500°C) for high-performance concrete. The effect of temperature on compressive strength, cubic compressive strength, cleavage strength, flexural strength, and the ultrasonic velocity of the high-performance concrete with fly ash was discussed according to the experimental results. The change of surface characteristics with the temperature was observed. It can serve as a reference for the maintenance, design, and the life prediction of high-performance concrete engineering, such as high-rise building, subjected to elevated temperatures.

1. Introduction

High-performance concrete (HPC) [1–5] is a complex system of materials that perform most effectively when placed in severely aggressive environments. It has found widespread usage in construction application including bridges, tunnels and high-rise building. Concrete in normal conditions is a versatile, resistant, and durable construction material. However under several physical and chemical processes as well as certain environmental conditions, it may deteriorate in a short period of time. As the use of high-performance concrete becomes common, the risk of exposing it to elevated temperatures also increases. The behavior of high-performance concrete under elevated temperatures differs from that of plain concrete. To be able to predict the response of structures employing high-performance concrete during and after exposure to high temperature, it is essential that the strength properties of high-performance concrete subjected to high temperatures should be clearly understood.

Fly ash (FA) is a byproduct of thermal power stations [6]. It is estimated that approximately 600 million tons of FA are available worldwide now, but at present, the current worldwide utilization rate of FA in concrete is about 10% [7]. FA is one of the most common concrete ingredients due to their pozzolanic properties [7, 8]. In the past two decades, considerable attention has been given to the use of FA as a partial replacement for cement in the production of high-performance concrete.

Kim et al. [9] studied the effect of elevated temperatures ranging from 20°C to 700°C on the mechanical properties of high-strength concrete of 40, 60, and 80 MPa grades. Poon et al. [10] investigated the effects of elevated temperatures on the compressive strength of fiber reinforced high-performance concrete. The results showed that, after exposure to 600 and 800°C, the concrete mixes retained, respectively, 45% and 23% of their compressive strength, on average. Khaliq and Kodur [11] present the effect of temperature on thermal and mechanical properties of high-performance self-consolidating concrete. In particular, there is a great risk that HPC spalls at elevated temperature compared with plain concrete [12, 13]. Due to the poor fire resistance of HPC [14, 15], it should be recommended that the use of HPC should be limited in some cases unless future research is carried out to study and solve this problem. Thus, the investigation on

Table 1: Mix proportions and major parameters of concrete.

Strength level	Cement (kg/m^3)	Sand (kg/m^3)	Coarse aggregate (kg/m^3)	Water (kg/m^3)	Fly ash (kg/m^3)	Water-reducing agent (kg/m^3)	Slump (cm)
C60	470	616	1095	175	94.5	6.77	24
C50	434	640	1080	185	91.0	5.81	25

performance of HPC subjected to elevated temperature is of great significance. This paper presents an experimental study of high-performance concrete with characteristic compressive strength of about 50 MPa and 60 MPa after 20°C, 200°C, 300°C, 400°C, and 500°C according to the GB/T 50081-2002 (standard for test method of mechanical properties on ordinary concrete) [16]. The compressive strength, cubic compressive strength, cleavage strength, flexural strength, and the ultrasonic velocity of HPC with fly ash were measured. The objective of this study is to increase the insight of the mechanical behavior of high-performance concrete with FA after exposure to elevated temperatures.

2. Experimental Procedures

2.1. Materials and Mix Proportions. To produce such a better quality of concrete, chemical and mineral admixtures such as fly ash, slag cement, and water reducers are commonly used in the field construction to increase the concrete strength. In this experimental study, two high performance concrete mixes have been studied, one high-performance concrete with a characteristic compressive strength of about 50 MPa, denominated C50, and another high-performance concrete, designed to achieve a compressive strength of about 60 MPa, denominated C60. In this experimental study, samples were made in a variety of trial concrete mix proportions and tested to determine the proportion which provided the required strength. Local materials were utilized. A Chinese standard (GB175-99) [17] 525 Portland cement (which has standard compressive strength of 52.5 MPa at the age of 28 days) was used. Natural river sand with fineness modulus of 2.6 was used. Coarse aggregate was a crushed stone with diameter from 5 mm to 20 mm. FA was applied to the mixture to the proportion of 20% (C50) and 21% (C60) of cement weight. Due to low water-cement ratios of the concrete mixtures, a water-reducing agent was employed. The mixture proportions and the major parameters for the two batches are listed in Table 1.

2.2. Samples and Testing Programs. In this study, all mixes were elaborated using a $0.25\,m^3$ horizontal forced action mixer. The mixing procedure was as follows: first the coarse aggregate, then fine aggregate, and the cement were loaded with the FA. These components were mixed for about 1 minute and after it the water with water-reducing agent was added in one minute and the mixing continued for another 3 minutes and the process finished.

Concrete prisms with size of 100 mm × 100 mm × 100 mm to determine the compressive strength (in order to eliminate the restraint on the loading surfaces, the friction-reducing pads were placed between the platens and the specimens for all tests. The pads consist of three plastic membranes with three layers of butter between them [18]), cubic compressive strength, cleavage strength, and the ultrasonic velocity and 100 mm × 100 mm × 400 mm to determine the flexural strength were casted in steel molds. During casting, compaction was achieved by placing the molds on a vibrating table and vibrating it at a frequency of 40 HZ for one second. All cast specimens were compacted through external vibration and demoulded 24 h later. Thereafter, all the specimens were cured in a moisture room with a condition of 20 ± 3°C and 95% RH for 27 days. At 28 days, the specimens were transported to the normal environment. At 120 days, the specimens were ground and prepared for testing. The two sides of specimen were ground to ensure that the specimen had flat edges and right angle corners. The final ground surface finish was within ±0.01 mm.

The tests of high temperatures were performed in the high temperatures testing apparatus in State Key Laboratory of Coastal and Offshore Engineering, Dalian University of Technology. The high temperatures testing apparatus was a box-type electric furnace, as shown in Figure 1. The 100 mm cubic specimens were elevated to the peak temperatures of 200°C, 300°C, 400°C, and 500°C at a heating rate of 10°C/min, respectively. Then 6 h was maintained after the peak temperature was reached. The cooling time in electric furnace was about 24 h, and then the specimens were taken out and cooled naturally to room temperature.

The compression testing machine used for this experiment was a machine with a maximum capacity of 100 KN, as shown in Figure 2. Compressive testing of the test specimens was done in accordance with (standard for test method of mechanical properties on ordinary concrete) GB/T 50081-2002 [16]. The maximum loading force was always applied to the surfaces that were perpendicular to the cast surfaces. The testing of the specimens can be carried out in stress-controlled mode, and all specimens were tested at a loading speed of 20.0 MPa per minute.

3. Results and Discussions

3.1. Failure Modes. Figures 3(a) and 3(b) show the failure modes of HPC under uniaxial compression with and without friction-reducing pads, respectively. The column-type fragments were observed for HPC under uniaxial compression with friction-reducing pads. The tensile strain will be caused in the direction of free surface because of the action of compressive load and the crack forms when the strain was larger than the ultimate tensile strain of the specimen. It was noticed that the cracks on the loaded surface have a random direction because of the influence of coarse aggregates.

Figure 1: Box-type electric furnace.

Figure 2: Compression testing machine.

The friction between loading plate and loading surface hinders the development of tensile strain close to loading surface. So the cracks will not form or the number of cracks will be reduced near the loading surface. The restriction effect of the friction between loading plate and loading surface on the development of tensile strain at the middle of the specimen is little. So the cracks near the middle of specimen will form. And the taper-type fragments were observed for HPC under uniaxial compression without friction-reducing pads.

The splitting tensile strain along the unload plane(s) was the cause of failure for both. It was obvious that the influence of elevated temperature on HPC did not change the tensile splitting mode from occurring. There was no great change in the failure modes for HPC after the action of elevated temperature.

Table 2: The cubic compressive strength of HPC at different ages (MPa).

Time (d)	3	7	14	21	28	60	90	120
C50	43.00	49.93	57.01	61.20	62.71	65.75	66.83	68.17
C60	46.73	54.27	61.97	66.52	68.17	71.47	72.64	74.10

Table 3: The compressive strength and cubic compressive strength of HPC at elevated temperature (MPa).

Concrete		Temperature (°C)				
		20	200	300	400	500
C50	f_c	33.93	33.6	36.0.7	29.33	26.53
	f_{cu}	55.16	54.40	54.67	52.00	44.37
C60	f_c	51.60	50.33	42.0	44.73	37.13
	f_{cu}	68.17	66.62	63.51	67.0	55.53

3.2. Strength

3.2.1. The Cubic Compressive Strength and Compressive Strength. The compressive stress was calculated by dividing the compressive load by the area of loading section (0.01 m^2). For each mixture, a minimum of three specimens were tested at 3, 7, 14, 21, 28, 60, 90, and 120 days. Tables 2 and 3 provide the basic physical properties cubic compressive strength and compressive strength for the high-performance concrete at different ages, respectively.

The C50 and C60 concrete developed a 3-day compressive strength of 43.0 MPa and 46.73 MPa, respectively. (These high values are mainly due to the high fineness of the cement used. However, the 3-day compressive strength of the concrete made with the fly ash is still adequate for most of the concrete structures for formwork removal at three days.) At 7 days, the compressive strength of the C50 concrete approached that of the control concrete (50 MPa), and at 14 days it (57.01 MPa) surpassed design value of strength (50 MPa). While for C60 concrete, the compressive strength surpassed design value of strength (60 MPa) at 21 days. In fact, the 28-day compressive strength of the C50 and C60 concrete was 22% and 11% higher than the design value of strength, respectively.

The variation of the cubic compressive strength and compressive strength with time for two types of high-performance concrete is shown in Figure 4.

The variation of the cubic compressive strength and compressive strength with temperature is given in Table 3 for two types of high-performance concrete. In two types of HPC, temperature has a slight bearing on the cubic compressive strength of concrete in the temperature range from 20°C to 300°C. Initially, as the temperature increased to 200°C, the strength decreased compared to the original strength. With further increase in temperature, the specimens recovered part of their strength at 300°C. The strength at 300°C is about 99.1% and 93.2% of the original strength (at 20°C) for C50 and C60, respectively. During the temperature range of 400°C to 500°C, the strength drops sharply, reaching a low level of 80.4% and 81.5% of initial strength for C50 and C60, respectively. The cubic compressive strength of HPC with temperature is shown in Figure 5.

(a) (b)

Figure 3: Failure modes of HPC under uniaxial compression.

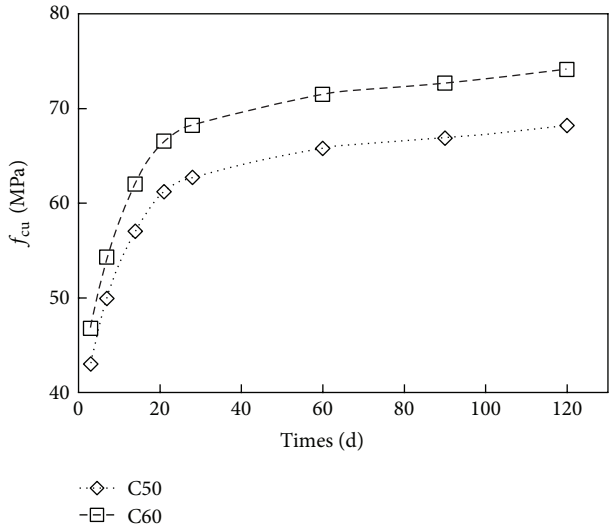

Figure 4: The variation of the cubic compressive strength with time.

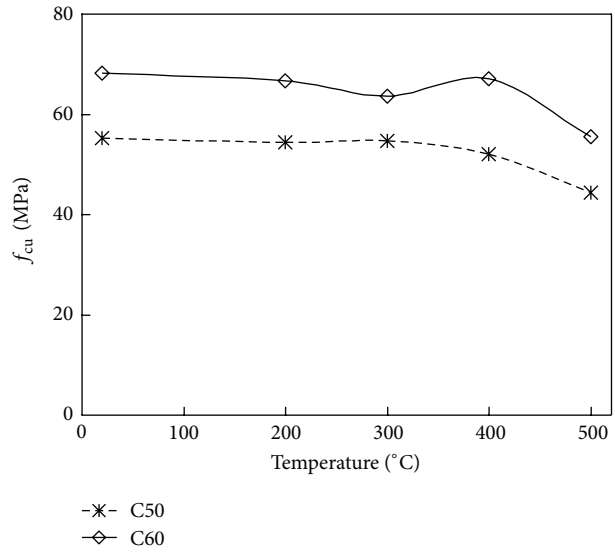

Figure 5: Cubic compressive strength of HPC at elevated temperature.

In the temperature range of 20°C to 200°C, the change of compressive strength is slight. Initially, as the temperature increased to 200°C, the strength decreased by 1.0% and 2.5% percent of the original strength. In the temperature range of 200°C to 300°C, the compressive strength of C50 increases to 1.06 times the original strength, while the compressive strength of C60 drops to 81.4% of the original strength. In the temperature range of 400°C to 500°C, all two types of HPC lose their strength at a faster rate, and the strength drops sharply, reaching a low level of 78.2% and 72.0% of initial strength for C50 and C60, respectively. At these temperatures, the dehydration of the cement paste results in its gradual disintegration. Since the paste tends to shrink and aggregate expands at high temperature (differential thermal expansion at temperatures above 100°C), the bond between the aggregate and the paste is weakened, thus reducing the strength of the concrete. Figure 6 gives the change of compressive strength of HPC with temperature. This was different from the result in [19]. The test results in [19] indicated that each temperature range had a distinct pattern of strength loss.

3.2.2. The Cleavage Strength and Flexural Strength. Cleavage strength and flexural strength of the concrete are given in Tables 4 and 5. The loading mode of cleavage test meeting (Testing Code of Concrete for Port and Waterwog Engineering) [20] was used. The 120-day cleavage strengths were 3.80 and 4.47 MPa for C50 and C60, respectively. The 120-day flexural strengths were 7.80 and 8.38 MPa for C50 and C60, respectively.

In the temperature range of 20°C to 200°C, temperature has a slight bearing on the cleavage compressive strength of two types of HPC concrete. The cleavage strength at 300°C

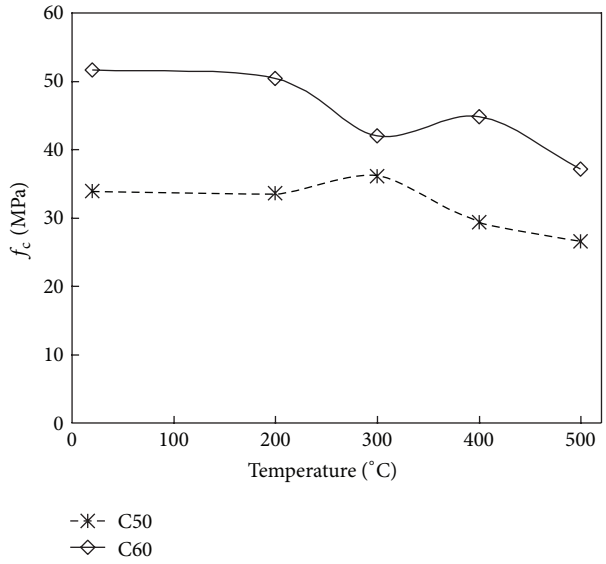

Figure 6: Compressive strength of HPC at elevated temperature.

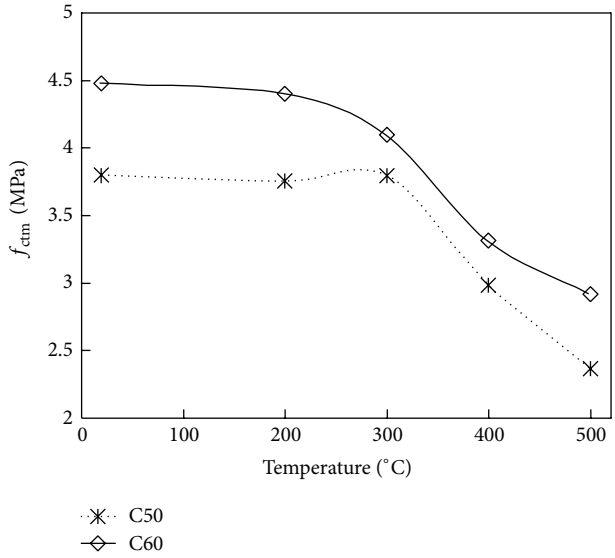

Figure 7: Cleavage strength of HPC at elevated temperature.

Table 4: The cleavage strength of HPC at elevated temperature (MPa).

Concrete	Temperature (°C)				
	20	200	300	400	500
C50	3.800	3.756	3.790	2.984	2.362
C60	4.474	4.401	4.098	3.310	2.916

Table 5: The flexural strength of HPC at elevated temperature (MPa).

Concrete	Temperature (°C)				
	20	200	300	400	500
C50	7.800	6.961	5.404	4.644	4.290
C60	8.380	8.253	6.565	5.834	5.378

of C50 and C60 is about 99.7% and 91.6% of the original strength (at 20°C), respectively. Above 300°C, the two types of HSC lose their cleavage strength at a faster rate. The cleavage strength at 500°C of C50 and C60 is about 62.2% and 65.2% of the original strength (at 20°C), respectively. The variation of the cleavage strength with temperature is shown in Figure 7.

Flexural strength is the most commonly used procedure to evaluate the toughness, and three-point bending tests are also carried out. For each mixture, the flexural strength was determined on two prisms each at elevated temperature (20, 200, 300, 400, and 500). In the temperature range of 20°C to 200°C, the change of fleural strength is slight. Initially, as the temperature increased to 200°C, the strength decreased 10.8% and 1.5% of the original strength for C50 and C60, respectively. As the temperature increased from 200°C to 500°C, the flexural strength dropped sharply compared to the original strength. Overall, HPC at elevated temperatures loses a significant amount of its compressive strength above 200°C and attains a strength loss of about 45.0% and 35.8%

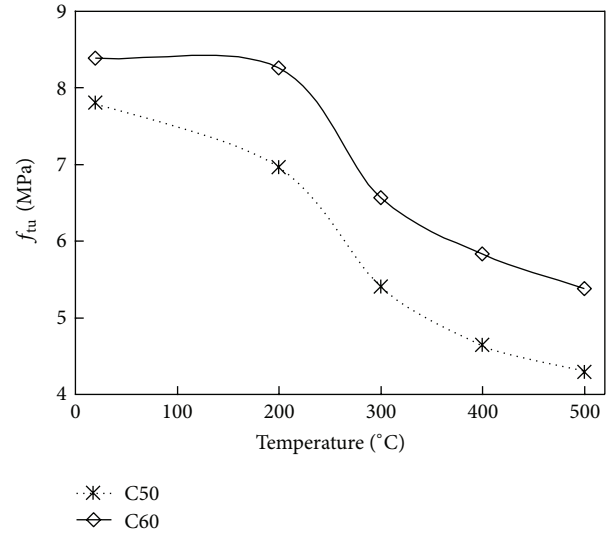

Figure 8: Flexural strength of HPCat elevated temperature.

at 500°C for C50 and C60, respectively. Figure 8 shows the flexural strength of HPC with elevated temperature.

3.3. The Ultrasonic Velocity. A lot of structures, like bridges, tunnels, dams, buildings, and others, were constructed with concrete material. During the life cycle of these structures, degradations can occur under mechanical, thermal, or chemical stresses. These often lead to the development of porosity, microcracks, and cracks in the material. Knowing the concrete structure state to prevent or repair damage is needed and so the nondestructive characteristic is an important stake, the ultrasonic method is often proposed. Ultrasound (sonic (frequency: from 20 to 20,000 Hz) human hearing range, subsonic (frequency: <20 Hz), and ultrasonic (frequency: >20,000 Hz)) is sound above the human hearing

Table 6: Loss of the ultrasonic velocity of HPC at elevated temperature.

Concrete	Temperature (°C)				
	200	300	400	500	500
C50	100	85.9	81.8	76.1	61.2
C60	100	92.2	80.8	69.3	58.5

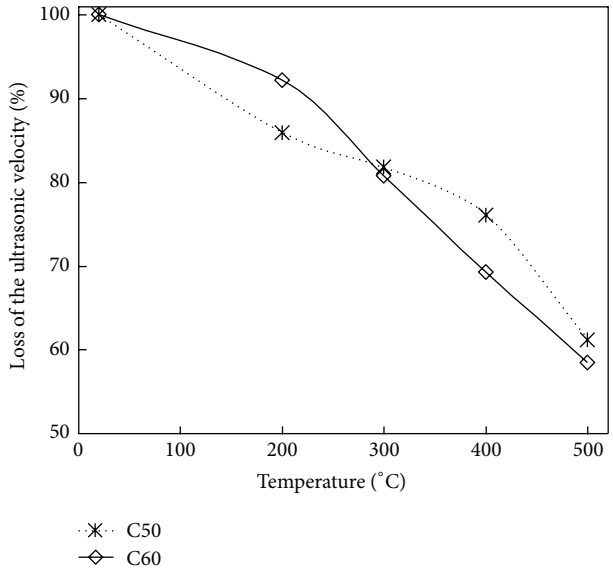

Figure 9: Loss of the ultrasonic velocity at elevated temperature.

range. Ultrasonic velocity is the speed in which sound travels through a given material. It is affected by density and elasticity. Velocity remains constant in a given material.

Table 6 gives the decreasing percentage of the ultrasonic velocity with temperature for high-performance concrete. As seen from Table 6 the ultrasonic velocity decreased as temperature. The ultrasonic velocity at 500°C of C50 and C60 is about 61.2% and 58.5% of the original velocity (at 20°C), respectively. Loss of the ultrasonic velocity of HPC with elevated temperature is shown in Figure 9.

3.4. The Surface Characteristics and Spalling. The induction of color change in concrete is associated with maximum temperature of exposure and loss in mechanical properties. By combining the changes of strength, color, and temperature during fire, the retained strength of concrete can be inferred primarily. This will provide some reference for concrete structure in practice. It can be said that, in the buildings damaged by fire, by examining the color of concrete surface, we can have some ideas about the change in the concrete strength [21]. So the change of color was observed; according to the visual inspection, a variation with color is revealed, and for concrete subject to 300°C, color does not change and it is gray, off-white when the concrete is exposed to temperature of between 400°C and 600°C.

Tanyildizi and Coskun [19] investigated the surface cracks; the results are as follows: the surface cracks started to appear at round 400°C, and continued to grow till the final rise in temperature up to 800°C. The crack decreased with the increase of fly ash content and at the same time increased with the increase of temperature. And no surface cracks were observed in the experiment.

However spalling has been identified as a problem with HPC by other researchers [22, 23]. But no evidence of spalling was founded during the simulated fire tests for HPC.

4. Conclusion

Based on the experimental work in this study and the discussion about test results, the following conclusions can be drawn

(1) The thermal properties, at elevated temperatures, exhibited by high-performance concrete are similar to those of plain concrete.

(2) The failure modes of HPC under uniaxial compression with and without friction-reducing pads were column-type fragments and taper-type fragments, respectively. The splitting tensile strain along the unload plane(s) was the cause of failure for both.

(3) Above 300°C, the two types of HSC lose their cleavage strength at a faster rate. The cleavage strength at 500°C of C50 and C60 is about 62.2% and 65.2% of the original strength (at 20°C), respectively. As the temperature increased from 200°C to 500°C, the flexural strength dropped sharply compared to the original strength.

(4) The present study was undertaken to establish the thermal properties of HPC at elevated temperatures. The data can be used to develop mathematical models to predict the fire resistance of HPC structural members.

Acknowledgments

This research work was jointly supported by the Science Fund for Creative Research Groups of the National Natural Science Foundation of China (Grant no. 51121005), the National Natural Science Foundation of China (Grant no. 51208273 and 51222806), a Project of Shandong Province Higher Educational Science and Technology Program (Grant no. J12LG07), and the Program for New Century Excellent Talents in University (Grant no. NCET-10-0287).

References

[1] S. Y. N. Chan, X. Luo, and W. Sun, "Effect of high temperature and cooling regimes on the compressive strength and pore properties of high performance concrete," *Construction and Building Materials*, vol. 14, no. 5, pp. 261–266, 2000.

[2] A. Neville and P. C. Aitcin, "High performance concrete-an overview," *Materials Structure*, vol. 31, pp. 111–117, 1998.

[3] M. Nehdi, S. Mindess, and P. C. Aïtcin, "Rheology of high-performance concrete: effect of ultrafine particles," *Cement and Concrete Research*, vol. 28, no. 5, pp. 687–697, 1998.

[4] Y. N. Chan, G. F. Peng, and M. Anson, "Spalling mechanism and fire resistance of high performance silica fume concrete with different moisture content," in *Proceedings of the 4th Beijing International Symposium on Cement and Concrete*, vol. 3, pp. 149–153, Beijing, China, 1998.

[5] J. Z. Xiao, P. Wang, J. Li, and S. D. Zhang, "Test on compressive strength of HPC with blast furnace slag after high temperature," in *Proceedings of the Fourth National Conference on HSC and HPC*, pp. 204–210, Changsha, China, 2001.

[6] R. Demirboğa, I. Örüng, and R. Gül, "Effects of expanded perlite aggregate and mineral admixtures on the compressive strength of low-density concretes," *Cement and Concrete Research*, vol. 31, no. 11, pp. 1627–1632, 2001.

[7] A. Bilodeau and V. M. Malhotra, "High-volume fly ash system: concrete solution for sustainable development," *ACI Structural Journal*, vol. 97, no. 1, pp. 41–48, 2000.

[8] A. Yeğinobalı, K. G. Sobolev, S. V. Soboleva, and B. Kıyıcı, "Thermal resistance of blast furnace slag high strength concrete cement," in *Proceedings of the 1st International Symposium on Mineral Admixtures in Cement*, pp. 106–117, Istanbul, Turkey, 1997.

[9] G. Y. Kim, Y. S. Kim, and T. G. Lee, "Mechanical properties of high-strength concrete subjected to high temperature by stressed test," *Transactions of Nonferrous Metals Society of China*, vol. 19, no. 1, pp. s128–s133, 2009.

[10] C. S. Poon, Z. H. Shui, and L. Lam, "Compressive behavior of fiber reinforced high-performance concrete subjected to elevated temperatures," *Cement and Concrete Research*, vol. 34, no. 12, pp. 2215–2222, 2004.

[11] W. Khaliq and V. Kodur, "Thermal and mechanical properties of fiber reinforced high performance self-consolidating concrete at elevated temperatures," *Cement and Concrete Research*, vol. 41, pp. 1112–1122, 2011.

[12] C. Castillo and A. J. Durrani, "Effect of transient high temperture on high-strength concrete," *ACI Materials Journal*, vol. 87, no. 1, pp. 47–53, 1990.

[13] G. Sanjayan and L. J. Stocks, "Spalling of high-strength silica fume concrete in fire," *ACI Materials Journal*, vol. 90, no. 2, pp. 170–173, 1993.

[14] C. Castillo and A. J. Durrani, "Effect of transient high temperature on high-strength concrete," *ACI Materials Journal*, vol. 871, pp. 47–53, 1990.

[15] J. Xiao and H. Falkner, "On residual strength of high-performance concrete with and without polypropylene fibres at elevated temperatures," *Fire Safety Journal*, vol. 41, no. 2, pp. 115–122, 2006.

[16] GB/T 50081-2002 and National Standard of the People's Republic of China, *Standard for Test Method of Mechanical Properties on Ordinary Concrete*, 2003.

[17] GB175-99 and National Standard of the People's Republic of China, *Portland Cement and Ordinary Portland Cement*, 1999.

[18] P. Y. Lu, Y. P. Song, and Z. M. Wu, "Strength and deformation characteristics of concrete subjected to different loading rates combined with confined stress," *Journal of Dalian University of Technology*, vol. 41, no. 6, pp. 716–720, 2001 (Chinese).

[19] H. Tanyildizi and A. Coskun, "The effect of high temperature on compressive strength and splitting tensile strength of structural lightweight concrete containing fly ash," *Construction and Building Materials*, vol. 22, no. 11, pp. 2269–2275, 2008.

[20] JTJ 270-98 and National Standard of the People's Republic of China, *Testing Code of Concrete for Port and Waterwog Engineering*, 1999.

[21] N. Yüzer, F. Aköz, and L. D. Öztürk, "Compressive strength-color change relation in mortars at high temperature," *Cement and Concrete Research*, vol. 34, no. 10, pp. 1803–1807, 2004.

[22] K. D. Hertz, "Danish investigations on silica fume concretes at elevated temperatures," *ACI Materials Journal*, vol. 89, no. 4, pp. 345–347, 1992.

[23] Y. N. Chan, G. F. Peng, and M. Anson, "Residual strength and pore structure of high-strength concrete and normal strength concrete after exposure to high temperatures," *Cement and Concrete Composites*, vol. 21, no. 1, pp. 23–27, 1999.

Hindawi Publishing Corporation
Advances in Materials Science and Engineering
Volume 2013, Article ID 809247, 7 pages
http://dx.doi.org/10.1155/2013/809247

Research Article

Feasibility of Pulverized Oyster Shell as a Cementing Material

Chou-Fu Liang and Hung-Yu Wang

Department of Civil Engineering, National Pingtung University of Science and Technology, 1 Hsuefu Road, Neipu, Pingtung 91201, Taiwan

Correspondence should be addressed to Hung-Yu Wang; hywang@mail.npust.edu.tw

Received 9 November 2012; Revised 27 February 2013; Accepted 4 March 2013

Academic Editor: Alex Li

This research intends to study the cementing potential of pulverized oyster shell, rich in calcium, when mixed with fly ash and soil. Cylindrical compacted soil and cubic lime specimens with different proportions of the shells and fly ash are made to study the strength variance. Soil, which is classified as CL in the USCS system, commercialized pulverized oyster shell, F-type fly ash, and lime are mixed in different weight percentages. Five sample groups are made to study the compressive strength of soil and lime specimens, respectively. The lime cubes are made with 0.45 W/B ratio and the cylindrical soils are compacted under the standard Procter compaction process with 20% moisture content. The results show that increment of shell quantity result to lower strength on both the soil and lime specimens. In a 56-day curing, the compressive strength of the lime cubes containing fly ash increases evidently while those carrying the shell get little progress in strength. The soil specimens containing fly ash gradually gain strength as curing proceeds. It suggests that mixtures of the shell and fly ash do not process any Pozzolanic reaction nor help to raise the unconfined strength of the compacted soil through the curing.

1. Introduction

Being an island, Taiwan is very rich in marine resources. Along the west coast of Taiwan, oyster farming is one of the most important production activities for the country's economy. In general, most of the oyster shells are discarded with no further use once the flesh is stripped off; except that a small amount is used for art creation [1, 2]. As a result, oyster shell piles are common in areas of oyster production with no further utilization. Chemical and microstructure analyses reveal that oyster shells are predominantly composed of CaO [3, 4], similar to that of lime, which has been used for soil stabilization [5]. In addition, oyster shells can be utilized for producing medium- and high-quality cement [6]. The expandable nature of clay is reduced by the ion exchange from the interaction between calcium ions and clay. Quicklime creates coagulation if added with water. Thus, calcium ions are used generally as the primary component in the clay stabilization. There is no known chemical reaction between soil and lime except the ion exchange. In other studies for potential use, the shells are mostly used as additive or replacement of part of the cement in concrete. For example, construction material mixed with crushed oyster shell and sand was used for sand compaction piles to improve soft soils underneath a breakwater port in Japan [7]. However, the lime contained in the shells does not provide improvement of concrete strength as the Pozzolanic products of concrete already contain lime, and therefore no positive effect is detected for concrete strength. According to [8], a pozzolan is defined as a siliceous and aluminous material, which in itself possesses little or no cementitious value but will, in finely divided form in the presence of moisture, chemically react with calcium hydroxide to form compounds possessing cementitious properties (Pozzolanic activity).

No concrete strength increase was found by adding sintered and pulverized oyster shells to concrete [9]. As a result, the use of pulverized oyster shells as concrete additive or cement replacement often needs to be combined with other bonding materials, such as fly ash or slag [8]. Only the Pozzolanic reaction between SiO_2 in the fly ash or slag and CaO in the pulverized oyster shells, along with the addition of water reducer or superplasticizer, can improve the strength of pulverized-oyster-shell-added concrete.

Table 1: Weight proportion of ingredients in cubic specimens.

Group	Lime	Fly ash	POS*
A	40	40	20
B	40	20	40
C	40	30	30
D	100	—	—
E	—	50	50

*Pulverized oyster shell.

Figure 1: Cubic specimens in the study.

Considering the scale of construction industries in the near future it is imperative to guarantee a secure supply of high-quality sand resources. Therefore, it is essential to conduct a research for other alternatives to meet future demands. Our research involves two major parts: first, the Pozzolanic reaction between F-type fly ash and the pulverized oyster shelland secondly, the improvement of soil strength, if the combination of pulverized oyster shells, clay, and sand can effectively improve the physical properties of soil such as strength [5, 6]. However, most of soil stabilization is done by in situ mixing, paving, and compacting. It is unlikely to obtain good control as it does in concrete mixing.

2. Specimens in the Tests

Lime cube specimens (125 cubic cm each) as illustrated by Figure 1 were made for testing the Pozzolanic potential of fly ash and oyster shell. There are five groups of cubic specimens with different proportions of lime, fly ash, and pulverized oyster shell. Each group contains 3 specimens. According to [10], using the water/cement ratio of 0.5, the comprehensive strength can reach 3000 psi (minimum comprehensive strength required for primary structures) for the replacement of percentage of oyster shell when it is 30%. To reach the same comprehensive strength for the water/cement ratio of 0.6, the replacement of oyster shell powder should be lower than 20%. For all mix designs, when the replacement percentage of oyster shell powder is 40%, the comprehensive strengths for them are all lower than 3000 psi. These render such concrete suitable for secondary structures. Hence, we choose W/B 0.45 and 40% weight of lime in the mixture of specimens. The lime is originally proposed to provide the adhesion for fixing the cubes, due to its low

Figure 2: Soil compaction mould assembly modified from concrete specimen mould.

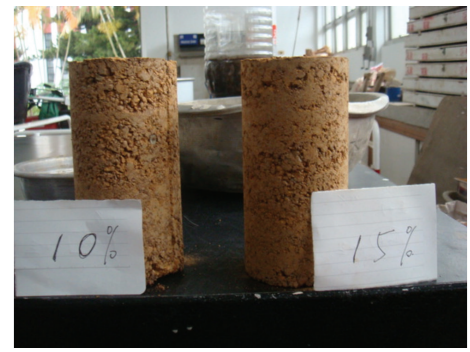

Figure 3: Compacted soil specimens.

strength after hardening, in case that the Pozzolanic reaction between fly ash and the oyster shell does not occur. However, the lime, when mixed with fly ash, becomes a main character providing the compressive strength of the cubes at the end of the study. The ratios of the ingredients, shown in Table 1, are chosen since the study mainly focuses on the reaction between fly ash and the shell, not the optimum ratio of the ingredients.

A USCS-classified CL soil is used in the compaction. The analysis of basic physical soil properties in the laboratory revealed that the plastic limit was 11% and liquid limit 25%, resulting in the plasticity index of 14%, which classifies the soil used to be low-plasticity soil according to the unified soil classification. The soil contained approximately 90% of fine particles, as the size of most particles was smaller than 2.75 mm (i.e., number 4 sieve). Only 2% of the particles were greater than 2.75 mm in size. The specific weight of soil particles was 2.63.

The Proctor (ASTM D698-12) standard compaction test was selected for soil dynamic analysis. Cylindrical soil specimens of $7.5\phi \times 15$ cm were prepared for unconfined compression test in order to find out the influence of pulverized oyster shells to the compression strength of soil. If the soil specimens were taken from the compacted soil in a standard compaction mould using thin tube, the sampling would create excessive disturbance affecting the test result. Considering the minimization of disturbance to soil specimens, the standard compact mould was not used for compaction in the specimen

Table 2: Weight percentage of ingredients used in soil specimens.

Group	Soil	Fly ash	POS*
A	100	—	—
B	95	—	5
C	85	—	15
D	95	5	—
E	85	7.5	7.5

*Pulverized oyster shell.

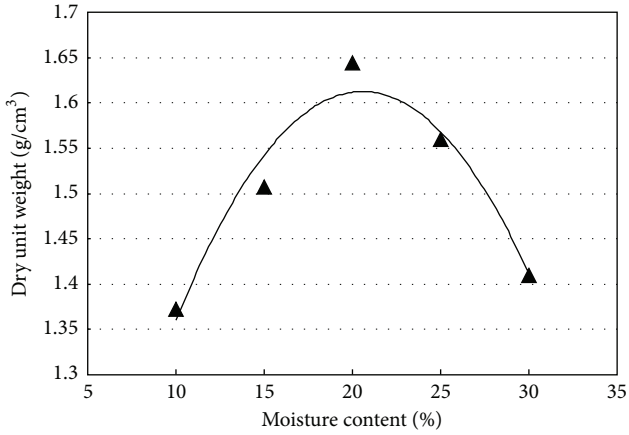

Figure 4: Compaction curve of soil group A.

preparation. Instead, a steel concrete specimen mould of $7.5\phi \times 15$ cm was chosen for compaction. Two steel moulds were connected with screws (Figure 2) to allow complete filling of soil in the mould. The number of hammering was calculated based on the compaction energy received per soil volume in the standard compaction test.

Specimens were produced with repeated compactions and 1.2 kg of soil was used to fill the mould in three layers. Eight compactions were exercised for every layer. Specimens were produced at a height of roughly 16 cm based on the soil weight and procedure. The part of soil hanging outside of the mould was carefully removed using a steel saw, thus resulting in cylindrical specimens of $7.5\phi \times 15$ cm (Figure 3) and eliminating the disturbance that sampling with thin tube would have caused, in the hope of minimizing test error.

Specimens were separated in 5 groups, in each of which different proportions in weight of pulverized oyster shells and fly ash were added in place of partial soil for specimen production. The purpose was to investigate the influence of pulverized oyster shells and fly ash to the compression strength of soil. The composition of each group is shown in Table 2. The compression test was carried out on days 7, 28, 60, and 90 to investigate the changes of unconfined compression strength at different days.

3. Water in the Compacted Soil

The maximum dry density of soil sample and the difficulty of removing the specimens from mould must be considered, as the specimens produced for the study were not made in the standard mould. The soil of each group was compacted according to the compaction energy and soil weight determined previously. The compaction result of some of the soil is shown in Figures 4, 5, and 6.

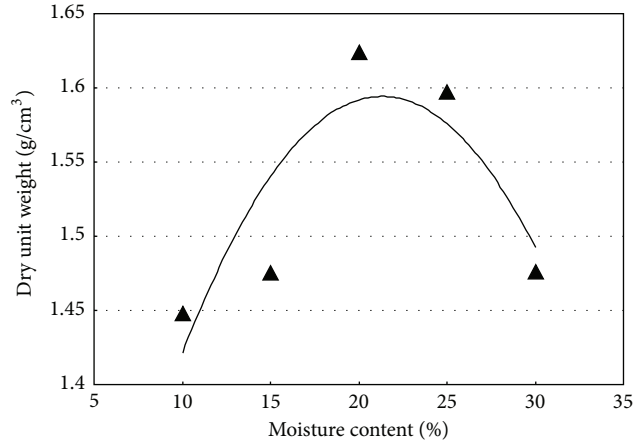

Figure 5: Compaction curve of soil group B.

From the above, it is found that the addition of pulverized oyster shells improved the optimal moisture content in the soil from 20% to nearly 25%. Therefore, the soil was less sensitive to water, allowing the increase of moisture in soil without making the soil too soft. As nonstandard procedure was adopted for the compaction test, it is necessary to consider how to keep the specimens intact when removing them from moulds, and the soil strength, as well as the test result, is susceptible to moisture content. By considering both factors above and conducting trial and error, it is realized that the easiest way is to remove the specimens from the moulds at the content of 20%. As a result, the moisture content of 20% was used for the compaction of specimens. The changes in the strength of each group of specimens at the maximum dry density are not covered in this study.

The wet specific weight of specimens obtained in the compaction test was calculated based on 30 specimens taken from each group and is shown in Table 3, which indicates that the homogeneity of the specimens produced was satisfying with the specific weight of all specimens at 2.04 g/cm^3 for maximum (Group A) and 1.87 g/cm^3 for minimum (group E). The error of the maximum and minimum specific weights of the soil specimens relative to the average specific weight felt between 2.27%~2.64% with the largest difference of 4.16% occurring in Group E. At a specific weight of 2.2, the addition of pulverized oyster shells decreased the specific weight of soil specimens, suggesting that the specific weight of soil specimens decreases with the increase of addition of pulverized oyster shells, dropping from 1.97 g/cm^3 for pure soil to 1.94 g/cm^3 with the difference in specific weight at only 1.8%.

4. Specimen Curing and Compression Test

To prevent water in the specimens from vaporizing, the specimens were wrapped in plastic film when produced

Table 3: Specific weights of soil specimens by group.

Project	Group				
	A	B	C	D	E
Average	1.97	1.97	1.94	1.97	1.95
Standard deviation	0.03	0.02	0.02	0.02	0.03
Maximum (homogeneous difference %)	2.04 (3.73)	2.02 (2.47)	1.99 (2.60)	2.01 (1.75)	2.01 (2.64)
Minimum (homogeneous difference %)	1.91 (3.24)	1.92 (2.43)	1.89 (2.27)	1.92 (2.64)	1.87 (4.16)

Table 4: Compressive strength of lime cubes.

Time (day)	Compressive strength (N/cm^2)				
	A	B	C	D	E
7	48.3	26.1	32.5	33.7	28.4
	54.5	23.9	33.0	33.0	25.8
	43.1	25.5	32.1	40.3	—
Average	48.6	25.2	32.5	35.7	27.1
8	192.5	29.7	63.2	46.0	34.2
	159.5	28.1	83.4	47.2	33.0
	221.8	17.1	—	40.6	—
Average	191.3	24.9	73.3	44.6	33.6
56	324.2	32.8	—	—	39.3
	402.0	44.3	122.1	37.8	35.8
	436.5	42.0	179.2	27.4	—
Average	387.6	39.7	150.7	32.6	37.6

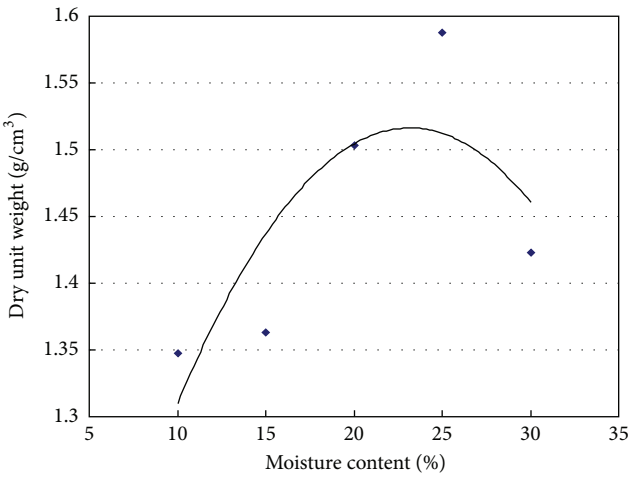

Figure 6: Compaction curve of soil group C.

Figure 7: Compacted soil specimens wrapped for curing.

(Figure 7) and placed in large plastic bags. Small amount of water was sprinkled in the plastic bags every week to keep the specimens properly moist, keeping in mind not to allow excessive moisture in them to ruin the result of compression test to come.

The unconfined compression test (i.e., the uniaxial compression strength test) was carried out at days 7, 28, and 75 of specimen curing to investigate the long-term influence of pulverized oyster shells and fly ash to the compression strength of compacted soil. The moisture content was measured after the compression test to determine the effect of the curing method on the moisture maintenance in soil.

5. Test Result

The lime cubes were then tested on the 7th, 28th, and 56th day. The results are shown in Table 4 and Figures 8 and 9. It shows that Pozzolanic reaction between fly ash and POS does not occur as expected. The strength of cube A gets higher as the curing time elapses, while cube E only gets slight increase in strength. It is reasonable to conclude that the strength of cube A is mainly gained from the Pozzolanic products from lime and fly ash. In addition, the compressive strength of the cubes is smaller as the weight percentage of pulverized oyster shell increases (Figure 9). The compressive strength of the D and E cubes eventually becomes the same

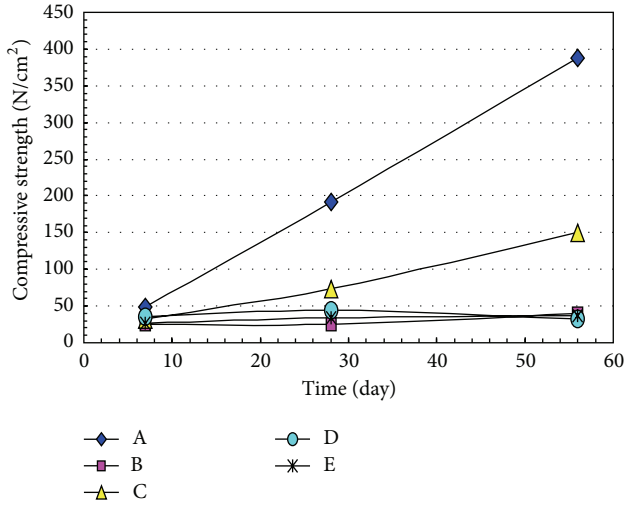

Figure 8: Strength development of lime cubes.

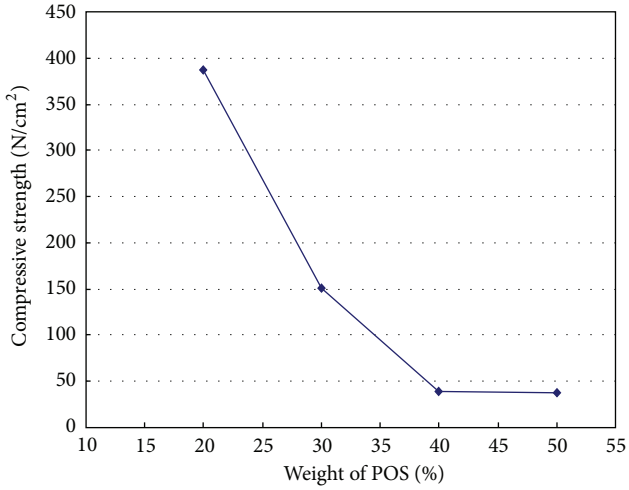

Figure 9: Strength of lime cubes versus weight percentage of pulverized oyster shell.

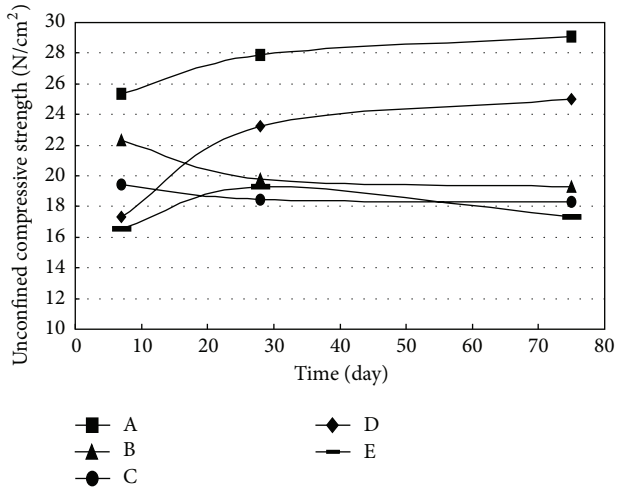

Figure 10: Unconfined strength of compacted soil.

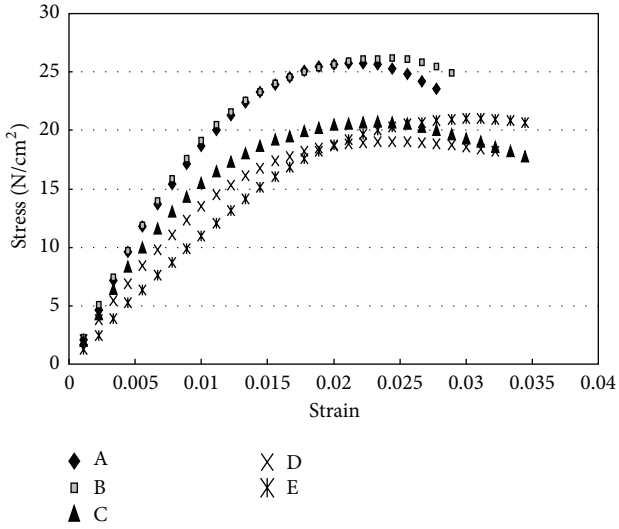

Figure 11: Stress and strain of the compacted soil at 7 days.

at any curing age. It suggests that, for the time being, the commercialized pulverized oyster will not have too much help in the Pozzolanic reaction with fly ash.

The compressive strength test on compacted soil specimens was scheduled at days 7, 28, 60, and 90. However due to equipment servicing, it was rescheduled at days 7, 28, and 75 of specimen age. Table 5 shows the strength of each group of specimens versus curing time, whereas Figure 6 gives the maxima of compression strength at each of the days.

From Tables 4 and 5 and Figure 10 above, it is clear that the addition of pulverized oyster shells gave no significant improvement for the compacted red soil taken from the National Pingtung University of Science and Technology campus in terms of the unconfined compression strength. The comparison of Groups A, B, C, and E in Figure 10 shows that the strength decreased significantly with the increasing addition. It is possible that no ion exchange occurred between the pulverized oyster shells chosen for this study and the clay, or the soil samples taken for this study might not be expansive, leading to no obvious iron exchange.

The addition of fly ash also led to decrease in the compression strength of the soil used in the study. However, its compression strength displayed a gradual increase. The addition of both pulverized oyster shells and fly ash in the soil did not provide the improvement in soil strength as the addition of only pulverized oyster shells did. It is concluded that the addition of both pulverized oyster shells and fly ash in Group E specimens did not improve the compression strength of soil by inducing the Pozzolanic reaction as expected.

Figures 11 and 12 show the stress-strain curves for each group of specimens at days 7, 28, and 75 in the compression strength test. The result suggests that the stress-strain curves become less steep with the decrease of strength. In addition, the compacted soil becomes soft and susceptible to displacement with the increasing addition of pulverized oyster shells.

Table 5: Unconfined compression strength of soil specimens for groups with different ages.

Time (day)	Compressive strength (N/cm^2)				
	A	B	C	D	E
7 days	22.1	23.5	20.7	15.6	21
	25.7	26.2	17.4	17.4	16.5
	28.2	17.2	20.2	19	12.2
Average	25.3	22.3	19.4	17.3	16.6
28 days	27.5	21	15.9	23.5	20.9
	29	17	17.5	22.8	19.4
	27.2	21.4	21.9	23.5	17.5
Average	27.9	19.8	18.4	23.3	19.3
75 days	28.1	19.6	16.8	21.6	17.5
	27.3	18.1	18.5	27.5	16.1
	31.9	20.1	19.6	25.9	18.4
Average	29.1	17.3	18.3	25	17.3

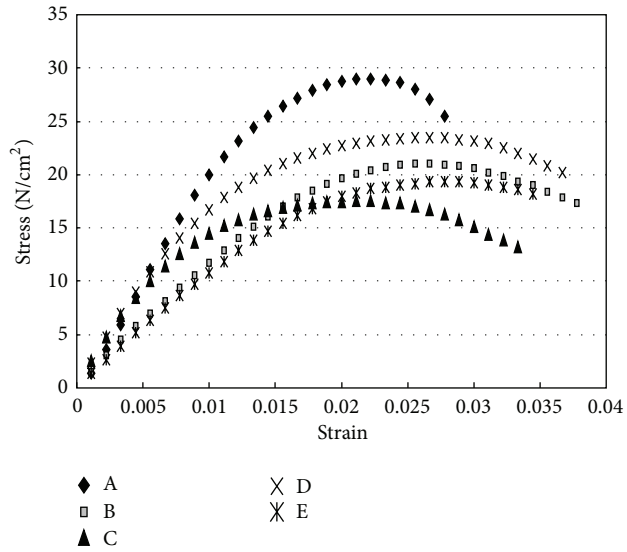

Figure 12: Stress and strain of the compacted soil at 28 days.

6. Conclusion and Suggestions

Standard moulds were not used for the compaction. However, the test result shows that the compaction is reasonable, and the specific weight of compacted soil suggests consistency of soil result. Therefore, the compaction selected for this study is feasible. The addition of pulverized oyster shells improves the optimal moisture content in the soil; that is, it decreases the sensitivity of soil to moisture content. However, at a specific weight of 2.2, the pulverized oyster shells do not improve the maximum dry density of the soil when added. The market-available pulverized oyster shells used in the study do not improve the compression strength of compacted soil in the experiment, and the drop of compression strength grows increasingly clear with the increase of addition. The test result suggests neither significant Pozzolanic reaction between the pulverized oyster shells used and the fly ash nor improvement of soil strength by adding both pulverized oyster shells and fly ash. The application of lime is a common and viable practice in soil stabilization and Pozzolanic reaction with fly ash. However, the strength improvement in compacted soil and lime blocks using lime-rich pulverized oyster shells perhaps is limited to the fineness and activity of pulverization, soil type, and aggregates. The same conditions do not apply to all test configurations. It is probably feasible to use pulverized oyster shells for their lime-rich nature in soil stabilization or in reaction with fly ash. However, the study did not yield the expected compressive strength increase in both compacted soil and lime blocks. How to improve the practicality of using pulverized oyster shells in soil stabilization remains to be investigated. The soil used in this study does not expand, resulting in lack of expected outcome. A test conducted on expandable clay may be considered to determine the suitability of pulverized oyster shells.

References

[1] "Fisheries Statistical Yearbook 1993–2001," Fisheries Agency, Council of Agriculture, Executive Yuan, Republic of China, http://www.fa.gov.tw/.

[2] "Study on the processing of waste oyster shells, National Taiwan Ocean University, Fisheries Bureau, Department of Agriculture and Forestry, Province of Taiwan," pp. 126–128, 1997.

[3] T. C. Chu, *Influence of replacement of cement and fine aggregates with waste pulverized oyster shells to the properties of cement mortar [M.S. thesis]*, Graduate Institute of Construction Engineering, National Yunlin University of Science and Technology.

[4] G. L. Yoon, B. T. Kim, B. O. Kim, and S. H. Han, "Chemical-mechanical characteristics of crushed oyster-shell," *Waste Management*, vol. 23, no. 9, pp. 825–834, 2003.

[5] M. G. Spangler and R. L. Handy, *Soil Engineering*, Harper & Row, 4th edition, 1982.

[6] B. Y. Zhong, Q. Zhou, C. F. Chan Y, and Y. Yu, "Structure and property characterization of oyster shell cementing material," *Chinese Journal of Structural Chemistry*, vol. 31, no. 1, pp. 85–92, 2012.

[7] Y. Miyaji and T. Okamura, "Geo-material properties of wasted oyster shell sand mixture and its application as material for sand

compaction pile," in *Proceedings of the Coastal Geotechnical Engineering in Practice*, pp. 675–680, Rotterdam, The Netherlands, 2000.

[8] V. G. Papadakis and S. Tsimas, "Supplementary cementing materials in concrete: part I. Efficiency and design," *Cement and Concrete Research*, vol. 32, no. 10, pp. 1525–1532, 2002.

[9] T. H. Wu, *Study on the stabilization of various roadbed soils using pulverized oyster shells [M.S. thesis]*, National Cheng Kung University, Taiwan, 2000.

[10] C. J. Lee, *A study on the application of oyster powder as a cementitious material [M.S. thesis]*, National Taiwan Ocean University, Taiwan, 2005.

Hindawi Publishing Corporation
Advances in Materials Science and Engineering
Volume 2013, Article ID 391957, 8 pages
http://dx.doi.org/10.1155/2013/391957

Research Article

Impact Behavior of Recycled Aggregate Concrete Based on Split Hopkinson Pressure Bar Tests

Yubin Lu,[1] Xing Chen,[2] Xiao Teng,[2] and Shu Zhang[2]

[1] *Key Laboratory of Testing Technology for Manufacturing Process (Ministry of Education), Southwest University of Science and Technology, Mianyang 621010, China*
[2] *School of Manufacturing Science and Technology, Southwest University of Science and Technology, Mianyang 621010, China*

Correspondence should be addressed to Yubin Lu; yubinluzju@hotmail.com

Received 7 November 2012; Revised 12 February 2013; Accepted 12 February 2013

Academic Editor: Alex Li

This paper presents the experimental results of recycled aggregate concrete (RAC) specimens prepared with five different amounts of recycled coarse aggregate (RCA) (i.e., 0, 25%, 50%, 75%, and 100%) subjected to impact loading based on split Hopkinson pressure bar tests. Strain-rate effects on dynamic compressive strength and critical strain of RAC were studied. Results show that the impact properties of RAC exhibit strong strain-rate dependency and increase approximately linearly with strain-rate. The transition point from low strain-rate sensitivity to high sensitivity decreases with the increase of matrix strength.

1. Introduction

The amount of construction and demolition waste (C&DW) has increased enormously over the last decade in the entire world. The recycling of waste concrete is beneficial and necessary for the environmental preservation and effective utilization of natural resources. The use of recycled coarse aggregate (RCA) obtained from C&DW in new concrete is a solution for the effective utilization of construction and demolition waste.

In practice, there are many incidents in which the structures undergo impact or explosion loading. The behavior of concrete structures subjected to dynamic loading is different from that under quasistatic loading. Due to the short duration of loading, the strain-rate of material is significantly higher than that under quasistatic loading conditions. Therefore, the present paper focuses on the behavior of recycled aggregate concrete (RAC) specimens prepared with different amounts of RCA under dynamic loading based on split Hopkinson pressure bar (SHPB) tests.

Many researchers have studied the dynamic behavior of plain, composite, and reinforced concrete specimens with natural coarse aggregates (NCA) based on SHPB tests. For example, Li and Xu [1] studied the impact mechanical properties of basalt fiber reinforced geopolymeric concrete based on a SHPB system; Rong et al. [2] investigated the dynamic compression behavior of ultrahigh performance cement based composites; Wang et al. [3] obtained the stress-strain relationship of steel fiber-reinforced concrete under dynamic compression based on SHPB. For RAC, Chakradhara Rao et al. [4] have studied its behavior under low velocity drop weight impact load. But no attempts have been made on the behavior of RAC specimens based on SHPB tests. Comparing with the drop weight impact technique, the SHPB technique has many advantages, like attaining higher striking velocities and thus higher strain-rates and can obtain stress-strain curves.

In this paper, the impact compression experiment is described in detail, including the preparation of RAC specimens and the SHPB test, in Section 2. Results of stress versus strain curves, failure patterns, strength, deformation, and energy absorption are presented and discussed in Section 3, followed by conclusions in Section 4.

2. Experiments

2.1. Materials. Raw materials used for RAC specimens are (1) RCA taken from waste concrete of a Mianyang road, the design strength of this waste concrete is unclear, and the waste concrete is broken by a jaw crusher, graded and cleaned to

Table 1: The mix proportions of RAC test specimens.

Mix designation	Cement	Water	Sand	NCA	RCA	Replacement ratio/%
PC-0	1	0.477	1.465	3.418	0	0
RC-25	1	0.477	1.465	2.564	0.854	25
RC-50	1	0.477	1.465	1.709	1.709	50
RC-75	1	0.477	1.465	0.854	2.564	75
RC-100	1	0.477	1.465	0	3.418	100

(a) Overall setup

Before impact After impact

(b) Specimen, incident, and transmitted bars

Figure 1: The 100-mm-diameter SHPB apparatus.

RCA of diameters from 10 to 20 mm; (2) NCAs are natural cobbles of diameters from 10 to 20 mm; (3) ordinary Portland cement of 42.5 grade is used; (4) fine aggregates are natural river sand of continuous grading with fineness modulus of 2.28; and (5) Mianyang tap water is used.

Concrete mix proportions largely influence the mechanical properties of concrete. To ensure the flowability during concreting and the strength after molding of RAC, the mix proportions of RAC specimens used in this study are cement : water : fine aggregate : coarse aggregate = 1 : 0.477 : 1.465 : 3.418, where coarse aggregates include NCA and RCA. According to the difference of replacement ratios of RCA, there are five different types of specimens, as shown in Table 1. PC-0 stands ordinary concrete specimens, and RC-25, RC-50, RC-75, and RC-100 stand RAC specimens with RCA replacement ratios of 25%, 50%, 75%, and 100%, respectively.

2.2. SHPB Tests. Dynamic compression tests of RAC are performed on 100 mm diameter SHPB setup with $\phi 100 \times 50$ mm cylinder specimens. The SHPB setup is shown in Figure 1. The length of the projectile, incident and transmission bar is 0.5, 4.5, and 2.5 m, respectively. The distance from the strain gauges on the incident bar and transmission bar and the interface of incident bar/specimen or specimen/transmission bar is 2.5 m and 0.5 m. The projectile, incident, and transmission bar are made of 48CrMoA and have Young's modulus of 210 GPa, density of 7850 kg/m^3, Poisson's ratio of 0.25–0.3, theoretical elastic wave velocity of 5172 m/s, and measured elastic wave velocity of 5200 m/s. The projectile bar is accelerated by the use of air pressure, and the projectile striking velocity is measured by laser velocimeter with the light distance of 0.1 m.

To ensure that the SHPB test results are valid, a critical condition that shall be satisfied is the stress equilibrium along the loading axial. Ravichandran and Subhash [5] proved that some time is needed for the specimen to achieve stress equilibrium state in the loading direction after it is first loaded, and this time is approximately $4\tau_s$ (where τ_s is the transit time for the leading edge of the stress pulse traveling through the specimen). Pulse shaping technique [6] can prolong the rise time of incident pulse, so that specimens have enough time to obtain stress equilibrium. Besides, it can smooth waveforms and eliminate waveform oscillations. In this study, for striking velocities <6 m/s, 6–10 m/s and 10–12 m/s, three different kinds of pulse shapers are used, that is, pasteboard of 0.67 mm thickness and 54.27 mm diameter, H62 brass of 1 mm thickness and 20 mm diameter, and H62 brass of 1 mm thickness and 30 mm diameter pulse shapers were, respectively, designed to improve incident waveforms. The quasistatic tensile stress-strain curves of standard H62 brass specimens are tested on a servohydraulic machine equipped with two cameras. Software based on a procedure called digital image correlation (DIC) was applied to process the images and subsequently determine the strains. Before

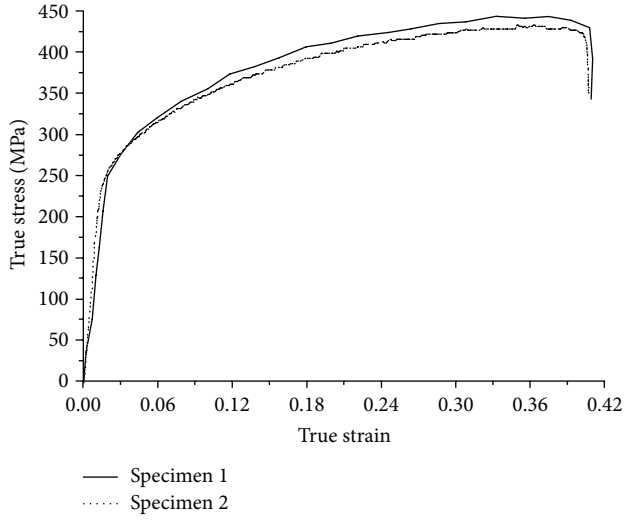

Figure 2: Quasi-static tensile stress-strain curves of H62 brass.

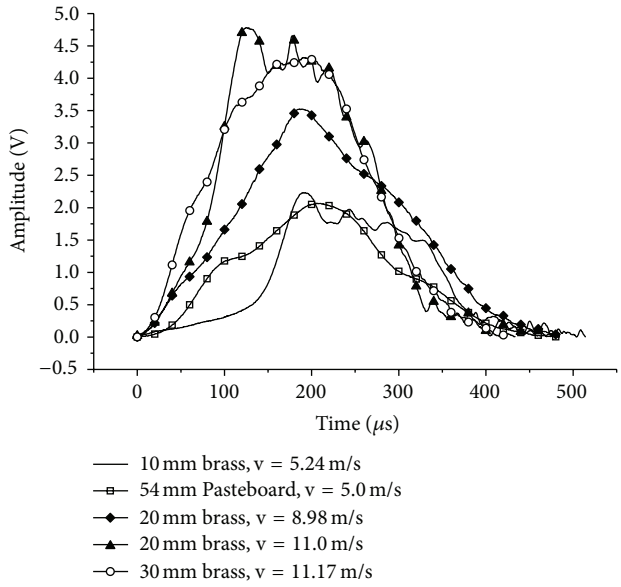

Figure 3: Incident waveforms shaped with different pulse shapers.

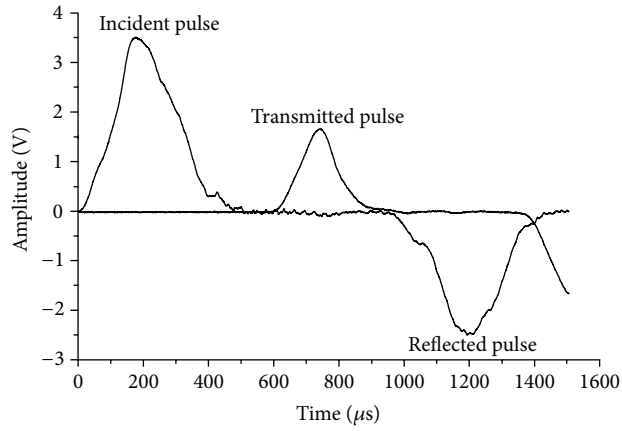

Figure 4: Incident, reflected, and transmitted waveforms shaped with a brass pulse shaper ($\phi 20 \times 1$ mm) for a NAC specimen under the striking velocity of 8.95 m/s.

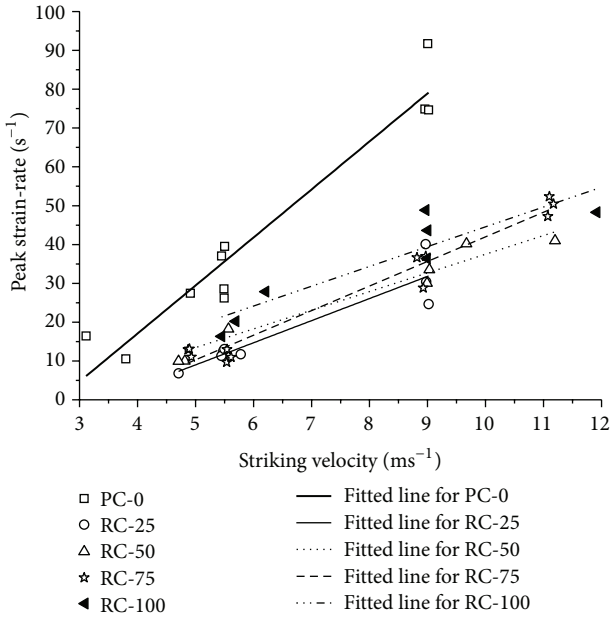

Figure 5: Peak strain-rate versus striking velocity with fitted lines.

each test, a random pattern with good contrast was applied to the surface of the specimen. This pattern deforms with the sample. The tensile stress-strain curves are shown in Figure 2. The Young's modulus is 100 GPa.

Figure 3 presents the comparison of shaped incident pulses by different pulse shapers. After using pulse shapers, the total duration of incident pulse is 433.5–514.5 μs and the rise time is up to 124.5–204.0 μs. Except the use of brass pulse shaper with 20 mm in diameter when the striking velocity is 11.0 m/s (the rise time is 124.5 μs), other pulse shapers provide sufficient time for the specimen to achieve stress equilibrium state in the loading direction. However, for low striking velocity (about 5 m/s), the shaped effect of pasteboard is better than that of brass with 10 mm in diameter. Figure 4 shows the typical incident, reflected and transmitted waveforms of a natural aggregate concrete (NAC) specimen shaped by a brass pulse with diameter of 20 mm. It shows that the dispersion of strain pulse during SHPB test is eliminated by the use of this pulse shaper.

In the study, various strain-rates were obtained by means of changing the projectile striking velocity. As shown in Figure 5, the relationship between the peak strain-rate $\dot{\varepsilon}_s$ (the strain-rate corresponding to the peak strength) and impact velocity v (m/s) can be approximately linearly expressed as

$$\dot{\varepsilon}_s = A + Bv, \tag{1}$$

where parameters A and B, together with the coefficients of determination R^2, for RAC specimens are summarized in Table 2. It is observed from Figure 5 that at the same striking velocity, the NAC specimens (PC-0) can attain higher peak

Table 2: Parameters in (1) for RAC specimens.

	PC-0	RC-25	RC-50	RC-75	RC-100
A	−32.41	−19.50	−10.59	−21.46	−6.51
B	12.37	5.70	4.81	6.35	5.10
R^2	0.92	0.84	0.95	0.96	0.78

strain-rate than RAC specimens (RC-25, RC-50, RC-75, and RC-100).

3. Experimental Results and Discussion

3.1. Stress versus Strain Curves and Failure Patterns. SHPB experiments were conducted at various strain-rates in the range of 10–100 s^{-1}. Average engineering stress $\sigma(t)$ on the two faces of the SHPB specimen and average engineering strain-rate $\dot{\varepsilon}(t)$ and strain $\varepsilon(t)$ over the length of the specimen are calculated from incident strain $\varepsilon_i(t)$, reflected strain $\varepsilon_r(t)$, and transmitted strain $\varepsilon_t(t)$ signals in the bars with three-wave method, that is,

$$\sigma(t) = \frac{A_b}{2A_s} E_b \left[\varepsilon_i(t) + \varepsilon_r(t) + \varepsilon_t(t)\right], \tag{2a}$$

$$\dot{\varepsilon}(t) = \frac{c_b}{L_s} \left[\varepsilon_i(t) - \varepsilon_r(t) - \varepsilon_t(t)\right], \tag{2b}$$

$$\varepsilon(t) = \frac{c_b}{L_s} \int_0^t \left[\varepsilon_i(t) - \varepsilon_r(t) - \varepsilon_t(t)\right] dt, \tag{2c}$$

where A_b, E_b, and c_b are the original cross-sectional area, Young's modulus, and elastic wave speed of the bars, respectively, and A_s and L_s are the original cross-sectional area and original length of the specimen, respectively. Stress versus strain curves obtained from SHPB tests are shown in Figure 6. The stress increases almost linearly initially and then decreases after the stress achieves the peak value. The strain-rate effect on the peak stress can be seen clearly.

Figure 7 presents the failure patterns of RAC specimens after impact under various striking velocities. However, to save the space, only typical photos are presented and others are omitted. It is observed that the failure pattern of RAC specimens is similar to that of NAC specimens. The impact failure becomes more and more violent and decisive with the increase of striking velocity. Under low striking velocity (i.e., <4 m/s), the RAC specimens are failed by the appearance of visible cracks. When the striking velocity is in the range of 4 and 6 m/s, the RAC specimens are failed by the disintegration of the tested cylinders mainly into big pieces. While the striking velocity is further increased, the RAC specimens fractured mainly in very fine fragments. For the striking velocity is over 11 m/s, many fine fragments are flown away such that only part failed specimens are recycled.

3.2. Strength. Figure 8(a) shows the dynamic compressive strength f_{cd} versus peak strain-rate for RAC specimens, which indicate that the impact properties of RAC are apparently strain-rate dependent and increase approximately linearly with the increase of peak strain-rate.

Table 3: Parameters in (3) for RAC specimens.

	PC-0	RC-25	RC-50	RC-75	RC-100
C	1.28	1.19	1.08	1.04	1.03
D	0.054	0.037	0.014	0.0074	0.0071
E	0.23	0.65	0.37	0.73	−0.25
F	1.31	0.57	0.26	0.40	1.00
$\dot{\varepsilon}_c$	6.65	10.40	11.75	6.65	19.95
R^2	0.64	0.74	0.57	0.29	0.82

It is believed that the dynamic increase factor (DIF) of concrete, which is the ratio of dynamic compressive strength to its corresponding quasi-static value, is directly dependent on the logarithm of the strain-rate. Therefore, the strain-rate dependence of DIF of RAC at strain-rates in the range of 10–100 s^{-1} can be defined as

$$\text{DIF} = \begin{cases} C + D\lg\left(\dot{\varepsilon}_s\right) & 10^{-5} \le \dot{\varepsilon}_s \le \dot{\varepsilon}_c\ s^{-1}, \\ E + F\lg\left(\dot{\varepsilon}_s\right) & \dot{\varepsilon}_c \le \dot{\varepsilon}_s \le 100\ s^{-1}, \end{cases} \tag{3}$$

where the parameter values of C, D, E, and F, together with the transition strain-rate $\dot{\varepsilon}_c$ from a low strain-rate sensitivity to a high sensitivity and the coefficients of determination R^2, are summarized in Table 3.

Equation (3), illustrated in Figure 9, clearly indicates that there is a sharp increase in DIF beyond the transition strain-rate of $\dot{\varepsilon}_c$ for RAC specimens. From Figure 9, it is found that DIF is reduced with the increase of RCA replacement ratio. When the strain-rates are over the transition strain-rate, the DIF of RAC specimens is largely smaller than that of NAC specimens.

3.3. Deformation. Critical compressive strain ε_c, which is defined as the stain when the stress reaches the peak, was used to describe the deformation property of RAC specimens. Bischoff and Perry [7] summarized a wide range of concretes of various quasi-static strengths and strain-rates, showing that significant increases in critical compressive strain were sometimes observed during impact loading, although these increases were generally less than those observed for strength. Figure 8(b) depicts a tendency that the critical compressive strain increases with the peak strain-rate, and the critical compressive strain of RAC specimens is smaller than that of NAC specimens. The relationship between critical compressive strain and peak strain-rate can be expressed as

$$\varepsilon_c = a + b\dot{\varepsilon}_s \tag{4}$$

in which the parameter values of a and b, and the coefficients of determination R^2, are summarized in Table 4.

3.4. Energy Absorption. Specific energy absorption U, which is expressed as the energy absorbed per unit volume of material [8], is used to describe the energy absorption property of RAC specimens and equals the area below the stress-strain curves. As shown in Figures 8(c)-8(d), specific energy absorption is 51.17–911.74 kJ/m^3 at peak strain-rate in the range of 10–100 s^{-1} and increases with the increase of

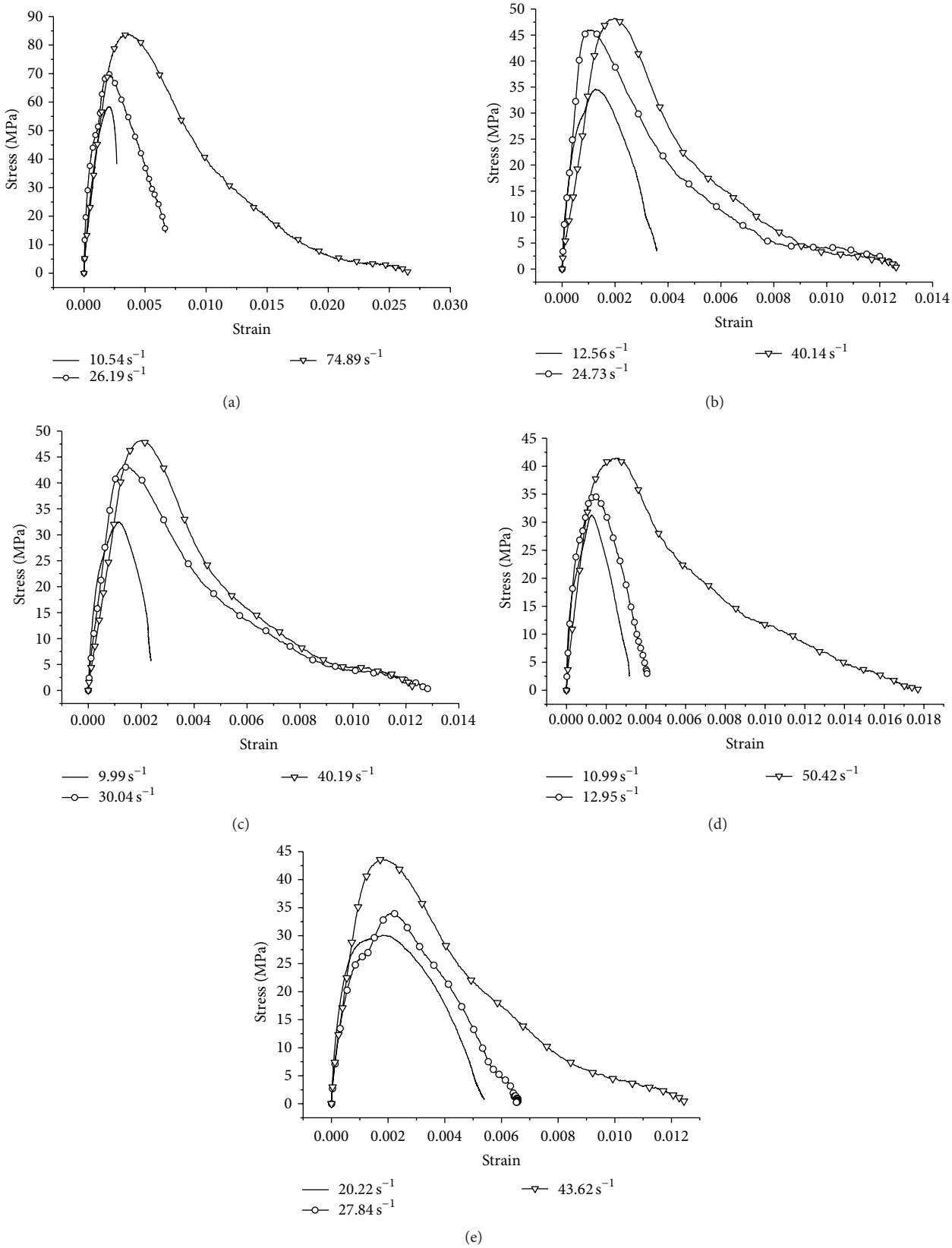

Figure 6: Stress versus strain curves of RAC specimens.

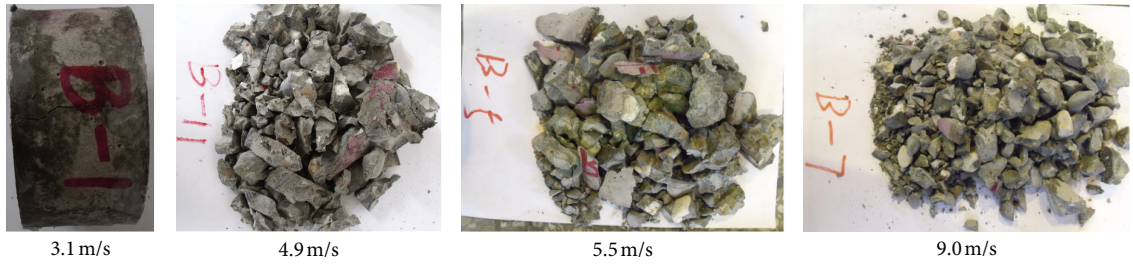

3.1 m/s 4.9 m/s 5.5 m/s 9.0 m/s

(a) PC-0

4.7 m/s 5.5 m/s 9.0 m/s

(b) RC-25

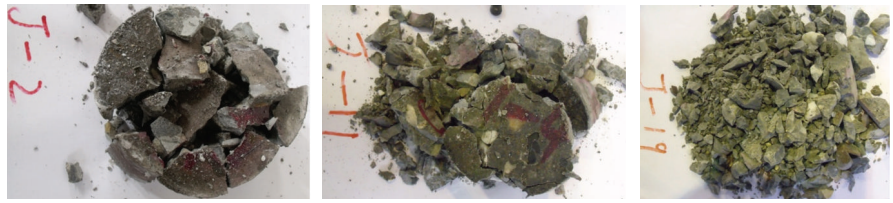

4.9 m/s 5.5 m/s 9.0 m/s

(c) RC-75

Figure 7: Failure patterns of RAC specimens under various striking velocities.

Table 4: Parameters in (4) for RAC specimens.

	PC-0	RC-25	RC-50	RC-75	RC-100
a	1.95	0.99	0.92	0.68	1.32
b	0.026	0.016	0.026	0.033	0.017
R^2	0.61	0.29	0.53	0.73	0.35

Table 5: Parameters in (5) for RAC specimens.

	PC-0	RC-25	RC-50	RC-75	RC-100
c	−72.78	−36.07	−14.22	8.99	−14.76
d	15.29	12.35	7.13	5.93	6.74
e	−0.048	−0.15	−0.015	−0.0079	−0.022
R^2	0.99	0.96	0.95	0.98	0.84

peak strain-rate. The relationship between the specific energy absorption and peak strain-rate can be expressed as

$$U = c + d\dot{\varepsilon}_s + e\dot{\varepsilon}_s^2 \quad (5)$$

in which the parameter values of c, d, and e, and the coefficients of determination R^2 are summarized in Table 5.

In addition, it can be seen in Figures 8(c)-8(d) that the specific energy absorption and its increase velocity of NAC specimens are largely greater than those of RAC specimens. Hence, the efficiency of absorbing impact energy of NAC specimens is higher than that of RAC specimens.

4. Conclusions

A 100 mm diameter SHPB system was used to investigate the mechanical properties of RAC specimens at high strain-rates in the range of 10–100 s^{-1}. The main conclusions can be drawn below.

(1) The impact properties of RAC specimens, including dynamic compressive strength, critical compressive strain, and specific energy absorption exhibit obvious strain-rate dependency and increase with the increase of peak strain-rate.

(2) The DIF of RAC specimens is reduced with the increase of RCA replacement ratio. When the peak strain-rates are over the transition strain-rate, the DIF of RAC specimens is largely smaller than that of NAC specimens.

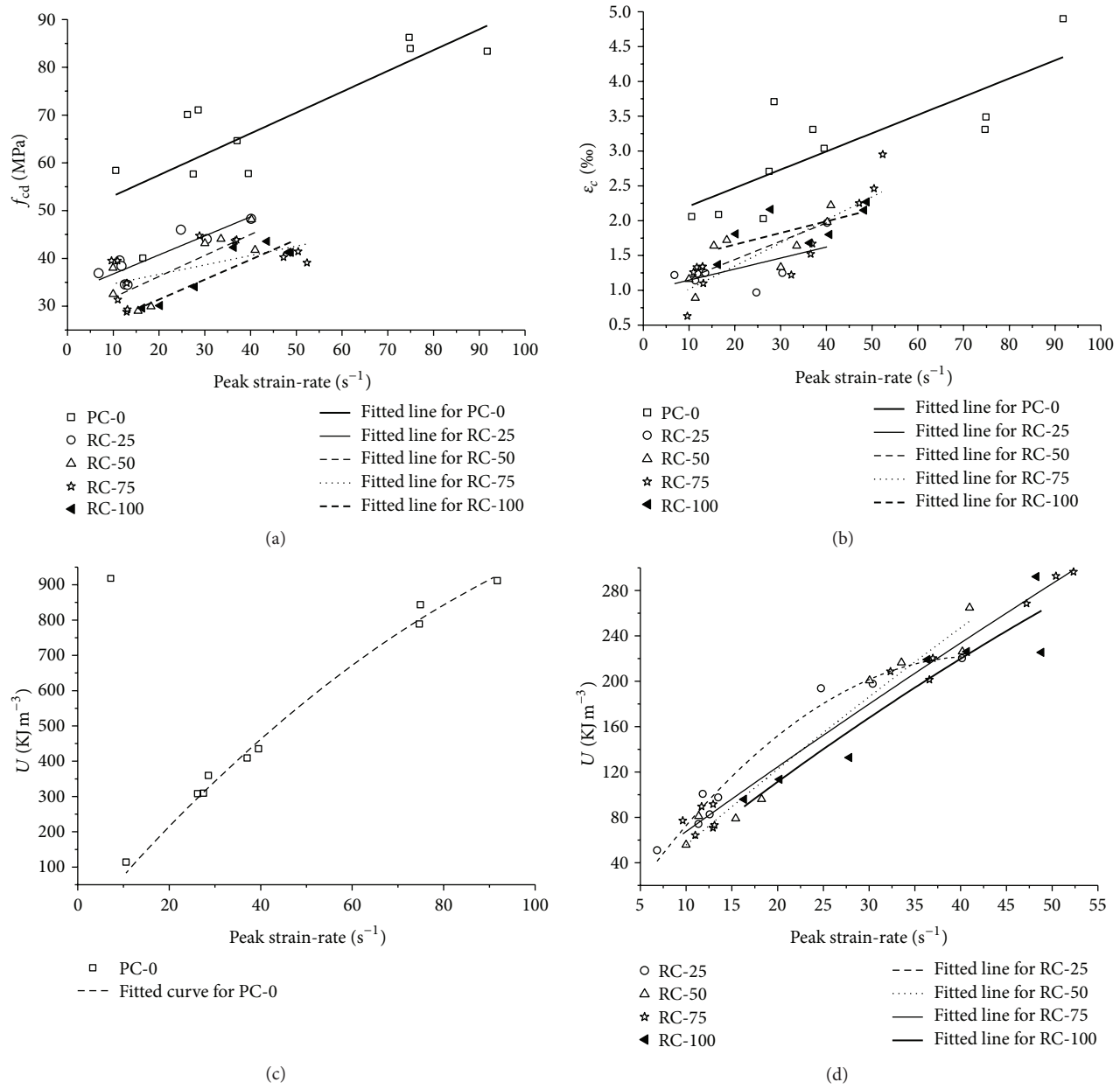

Figure 8: Dynamic compressive strength and critical compressive strain versus peak strain-rate for RAC specimens.

(3) The critical compressive strain of RAC specimens is smaller than that of NAC specimens. Thus, the deformation capacity of RAC specimens is weaker than that of NAC specimens.

(4) The specific energy absorption and its increased velocity of NAC specimens are largely greater than those of RAC specimens. Hence, the energy absorption capacity of RAC specimens is lower than that of NAC specimens.

Besides, as this study shows that the dynamic compressive properties of RAC are much inferior to those of NAC, and most of the dynamic compressive properties deterioration of RAC is exhibited between 0% and 25% of the replacement ratio, while up to 100% of the replacement ratio the deterioration is not so severe. To further explain these phenomena and improve the dynamic behavior of RAC, following studies are ongoing by the use of microscopic approaches to investigate the effect of RCA and interfacial transition zone on RAC dynamic properties.

Acknowledgments

The First author would like to acknowledge the support by the Open Project of State Key Laboratory Cultivation Base for Nonmetal Composites and Functional Materials (10zxfk06)

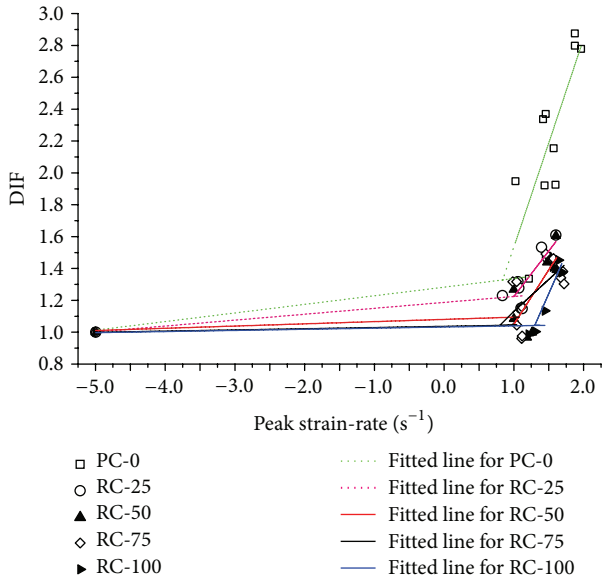

Figure 9: Relationships between DIF and peak strain-rate for RAC specimens.

and the Doctorate Foundation of Southwest University of Science and Technology (10zx7141).

References

[1] W. Li and J. Xu, "Mechanical properties of basalt fiber reinforced geopolymeric concrete under impact loading," *Materials Science and Engineering A*, vol. 505, no. 1-2, pp. 178–186, 2009.

[2] Z. Rong, W. Sun, and Y. Zhang, "Dynamic compression behavior of ultra-high performance cement based composites," *International Journal of Impact Engineering*, vol. 37, no. 5, pp. 515–520, 2010.

[3] Z. L. Wang, Y. S. Liu, and R. F. Shen, "Stress-strain relationship of steel fiber-reinforced concrete under dynamic compression," *Construction and Building Materials*, vol. 22, no. 5, pp. 811–819, 2008.

[4] M. Chakradhara Rao, S. K. Bhattacharyya, and S. V. Barai, "Behaviour of recycled aggregate concrete under drop weight impact load," *Construction and Building Materials*, vol. 25, no. 1, pp. 69–80, 2011.

[5] G. Ravichandran and G. Subhash, "Critical appraisal of limiting strain rates for compression testing of ceramics in a split Hopkinson pressure bar," *Journal of the American Ceramic Society*, vol. 77, no. 1, pp. 263–267, 1994.

[6] Y. B. Lu and Q. M. Li, "Appraisal of pulse shaping technique in split Hopkinson pressure bar tests for brittle materials," *International Journal of Protective Structures*, vol. 1, no. 3, pp. 363–390, 2010.

[7] P. H. Bischoff and S. H. Perry, "Compressive behaviour of concrete at high strain rates," *Materials and Structures*, vol. 24, no. 6, pp. 425–450, 1991.

[8] T. X. Yu and G. X. Lu, *Energy Absorption of Structures and Materials*, Chemical Industry Press, Beijing, China, 2005.